










# LARP6C orchestrates posttranscriptional reprogramming of gene expression during hydration to promote pollen tube guidance

Elodie Billey <sup>1,2,†</sup> Said Hafidh <sup>3,\*</sup> Isabel Cruz-Gallardo <sup>4,§</sup> Celso G. Litholdo Jr,<sup>1,2</sup> Viviane Jean,<sup>1,2</sup> Marie-Christine Carpentier <sup>1,2</sup> Claire Picart,<sup>1,2</sup> Vinod Kumar <sup>3</sup> Katarina Kulichova,<sup>3</sup> Eric Maréchal,<sup>5</sup> David Honys <sup>3</sup> Maria R. Conte <sup>4</sup> Jean-Marc Deragon <sup>1,2,6,\*</sup> and Cécile Bousquet-Antonelli <sup>1,2,\*,†</sup>

- 1 Laboratoire Génome et Développement des Plantes, UMR5096, CNRS, 66860 Perpignan, France
- 2 Laboratoire Génome et Développement des Plantes, UMR5096, Université de Perpignan Via Domitia, 66860 Perpignan, France
- 3 Laboratory of Pollen Biology, Institute of Experimental Botany of the Czech Academy of Sciences, 16502 Prague 6, Czech Republic
- 4 Randall Centre for Cell and Molecular Biophysics, King's College London, London SE1 1UL, UK
- 5 Laboratoire de Physiologie Cellulaire et Végétale, UMR 5168 CNRS, CEA, INRAE, Université Grenoble Alpes, IRIG, CEA Grenoble, 38054 Grenoble, France
- 6 Institut Universitaire de France, 75231 Paris Cedex 5, France

\*Author for correspondence: cecile.antonelli@univ-perp.fr (C.B.-A.), hafidh@ueb.cas.cz (S.H.), jean-marc.deragon@univ-perp.fr (J.-M.D.).

†Senior author.

‡Present address: TOTAL RC, 2 Place Jean Millier-Arche Nord Coupole/Regnault, 92078 Paris La Défense Cedex, France.

§Present address: Department of Chemistry, King's College London, Britannia House, 7 Trinity St, London SE1 1DB, UK.

These authors contributed equally (E.B., S.H.).

E.B. and S.H. performed the experiments and analyzed the data. C.P. helped E.B. with confocal microscopy analyses. V.J. helped E.B. with plant maintenance and reciprocal crossed. M.C.C. performed RNA-seq and RIP-seq bioinformatics. V.K. and K.K. assisted S.H. with in vitro pollen tube assays, and V.K. assisted S.H. with experiments presented in Figure 9. I.C.G. and M.R.C. designed and analyzed EMSA and ITCs; I.C.G. performed the experiments. C.G.L. Jr ran experiments from Figure 8. E.M. contributed his knowledge on lipid metabolism and suggested a role for MGD2 as cargo for TAGs. C.B.A. coordinated the work, designed the research, analyzed the data, and wrote the paper. J.M.D. helped with data analysis. E.B., S.H., M.R.C., J.M.D., and D.H. revised the manuscript.

The authors responsible for distribution of materials integral to the findings presented in this article in accordance with the policy described in the Instructions for Authors (<https://academic.oup.com/plcell>) are: Cécile Bousquet-Antonelli (cecile.antonelli@univ-perp.fr), Said Hafidh (hafidh@ueb.cas.cz), and Jean-Marc Deragon (jean-marc.deragon@univ-perp.fr).

## Abstract

Increasing evidence suggests that posttranscriptional regulation is a key player in the transition between mature pollen and the progamic phase (from pollination to fertilization). Nonetheless, the actors in this messenger RNA (mRNA)-based gene expression reprogramming are poorly understood. We demonstrate that the evolutionarily conserved RNA-binding protein LARP6C is necessary for the transition from dry pollen to pollen tubes and the guided growth of pollen tubes towards the ovule in *Arabidopsis thaliana*. In dry pollen, LARP6C binds to transcripts encoding proteins that function in lipid synthesis and homeostasis, vesicular trafficking, and polarized cell growth. LARP6C also forms cytoplasmic granules that contain the poly(A) binding protein and possibly represent storage sites for translationally silent mRNAs. In pollen tubes, the loss of LARP6C negatively affects the quantities and distribution of storage lipids, as well as vesicular trafficking. In *Nicotiana benthamiana* leaf cells and in planta, analysis of reporter mRNAs designed from the LARP6C target *MGD2* provided evidence that LARP6C can shift from a repressor to an activator of translation when the pollen grain enters the

## IN A NUTSHELL

**Background:** In flowering plants, pollen delivers male genetic material into the ovule, which is embedded in the pistil. When mature, the pollen dehydrates, turning “dormant”, with most of its cellular activities shutdown. Upon landing on a pistil, the pollen rehydrates and “awakens”; it germinates and grows a protrusion, the pollen tube, which elongates and navigates into the pistil guided by ovule-emitted signals, a process known as “pollen tube guidance”. Dormant pollen contains mRNAs encoding proteins stored as translationally silent. When the pollen “awakens”, translation is reactivated, which is crucial for the emergence of pollen tubes and their penetration into the pistil.

**Question:** How are mRNAs chosen to be stored? How do they reenter translation? Which proteins are involved in this process? We previously proposed that *Arabidopsis thaliana* LARP6C regulates mRNAs through direct binding, but we did not know which mRNAs it controls, how this occurs, and what purpose it serves in plant development. Since LARP6C is a pollen-specific protein, we studied its roles in plant reproduction.

**Findings:** Using *Arabidopsis* mutants, we show that pollen deprived of LARP6C has delayed germination and guidance defects. By binding to and regulating a precise subset of mRNAs, LARP6C controls lipid biology and vesicular trafficking in pollen tubes. The misregulation of these processes in *lar6c*-depleted pollen is likely the basis of their germination and guidance defects. Exploring how LARP6C regulates its mRNA targets, we discovered that this two-faced protein acts as a translational repressor in dormant pollen and an activator when the pollen “awakens”. However, things are not so simple as this: successful pollen tube guidance is seemingly dependent upon the two faced-nature that LARP6C retains in elongating pollen tubes.

**Next steps:** Next, we will seek to understand how LARP6C shifts from a repressor to an activator of translation when pollen exits its dormant state. This work also opens the possibility that the guidance process requires that some mRNAs are only reactivated translationally when they reach a precise subcellular location in the pollen tube. With LARP6C likely being part of this mechanism, we have a unique opportunity to explore this model.

progamic phase. We propose that LARP6C orchestrates the timely posttranscriptional regulation of a subset of mRNAs in pollen during the transition from the quiescent to active state and along the progamic phase to promote male fertilization in plants.

## Introduction

In the cytoplasm, messenger RNAs (mRNAs) coated with RNA-binding proteins (RBPs) in the form of ribonucleoprotein particles (mRNPs) are in balance between translation, storage, and decay. Translationally silent mRNPs can be stored and protected from decay in cytosolic aggregates and released when their protein product is needed. In response to developmental or environmental cues, the fine-tuning between mRNA decay rate or storage will have a direct impact on translation and hence gene expression. RBPs play a crucial role in this fine-tuning, enabling gene-specific regulation through binding to their mRNA targets.

LA and related proteins (LARPs) form a large family of eukaryote RBPs that share the La motif (LAM), a structured RNA-binding domain. LARPs are classified into five distinct subfamilies, including the LARP6 group (Bousquet-Antonelli and Deragon, 2009). In most LARPs, an RNA recognition motif (RRM1) is found immediately after the LAM and forms a bipartite RNA-binding unit called the La-module (Maraia et al., 2017). Although the LAM is usually very well conserved between subfamilies, the RRM1s are specific to each subgroup (Bousquet-Antonelli and Deragon, 2009;

Maraia et al., 2017). Members of the LARP6 subfamily are found in Stramenopiles, Chlorophytes, plants, invertebrates, and vertebrates and are characterized by the La-module and by a short conserved motif known as LAM and S1 Associated (LSA) at the C-terminus (Bousquet-Antonelli and Deragon, 2009) that mediates protein–protein interactions (Weng et al., 2009; Cai et al., 2010b; Vukmirovic et al., 2013; Manojlovic et al., 2017).

In mammals, one of the functions of LARP6 is to regulate the synthesis of type I collagen, a heterotrimer composed of two  $\alpha 1$  and one  $\alpha 2$  subunits whose assembly and correct secretion are dependent upon the coordinate translation of their transcripts at the endoplasmic reticulum (ER; Zhang and Stefanovic, 2016). The expression of type I collagen is primarily regulated by the binding of LARP6 through its La-module to a stem loop in their 5′-untranslated regions (UTRs; Cai et al., 2010a; Martino et al., 2015). LARP6 either stores or stabilizes the collagen mRNA transcripts in a translationally silent form by tethering them to vimentin filaments where they can further be activated for translation or subjected to decay (Challa and Stefanovic, 2011). Alternatively, LARP6 docks the mRNAs to nonmuscle

myosin filaments (Cai et al., 2010b; Manojlovic et al., 2017) and either recruits serine threonine kinase receptor associated protein (Vukmirovic et al., 2013) or RNA helicase A via its LSA (Manojlovic et al., 2017), which respectively function as a repressor and activator of translation. Through this mechanism, LARP6 orchestrates the coordinated translation of  $\alpha 1$  and  $\alpha 2$  collagen transcripts at the ER. More recently, human LARP6 was found to regulate the localization and translation of ribosomal protein (RP) mRNAs to cell protrusions, enhancing RP synthesis, ribosome biogenesis, and overall protein synthesis in migratory cells (Dermitt et al., 2020). Furthermore, in zebrafish (*Danio rerio*), both LARP6 paralogs are required for normal oocyte development, chorion formation, and egg activation (Hau et al., 2020).

While LARP6 proteins are generally encoded by a single gene, vascular plant proteins are encoded by three to six genes and are of three evolutionary types named 6A, 6B, and 6C (Merret et al., 2013b). While the members of 6A subgroup most closely resemble LARP6 from other eukaryotes, in addition to a reorganized La-module, B- and C-type orthologs carry a poly(A) binding protein (PABP)-interacting motif 2 (PAM2). *Arabidopsis thaliana* has three AtLARP6 genes, one of each type, which we will refer to as LARP6A, B, and C throughout this manuscript.

We previously demonstrated that LARP6C directly associates with the PABP in plants, which is consistent with the presence of a PAM2 motif and that the finding that its La-module binds to oligo( $U_{20}$ ) homopolymers in vitro. In addition, in onion (*Allium cepa*) epidermis, LARP6C accumulates in the cytoplasm, the nucleoplasm, and the nucleolus. Strikingly, LARP6C redistributes to stress granules upon hypoxia, where it associates with mRNP aggregates (Merret et al., 2013b). These data support the view that Arabidopsis LARP6C is an RBP that is likely involved in mRNA posttranscriptional regulation.

In flowering plants, the haploid male gamete (pollen grain) consists of a vegetative cell that encases two sperm cells, which are connected (through a so-called cytoplasmic connexion) with the vegetative cell nucleus to form the male germ unit. A characteristic feature of angiosperm sexual reproduction is that sperm cells are nonmotile and must be carried simultaneously to the ovule by a pollen tube (Johnson and Preuss, 2002). Upon adhesion to the stigma, the male vegetative cell hydrates, germinates, and grows into a tube that delivers the two sperm cells to the ovule. The pollen tube is a highly polarized and fast tip-growing cell whose growth directionality is determined by various perceived cues. It is first guided in the gynoecium by female sporophytic tissue in the pistil (preovular guidance) and then, upon exit from the transmitting tract, it navigates in gametophytic tissues guided by ovule-emitted signals (ovular guidance). Ovular cues guide the pollen tube alongside the funiculus to the micropyle. Upon reaching the ovule, the pollen tube stops growing and bursts to free the sperm cells that will fuse respectively with the egg cell (to form the embryo) and the central cell (to form the endosperm), hence completing the fertilization process (Higashiyama and Takeuchi, 2015).

In the pollen tube, upon reception and transduction of extracellular female signals, a complex cellular process targets the cell wall synthesis machinery at the site of perception, hence, permitting the delivery of macromolecules at site of extension and the directional growth of the tube. This requires tip-localized receptors, the flow of ions, intracellular trafficking of signaling molecules and proteins, and also vesicular trafficking, cytoskeleton-dependent transport, and novel cell wall formation through exocytosis (Hafidh et al., 2014; Higashiyama and Takeuchi, 2015; Feng et al., 2018). Pollen tube growth also requires changes in the pattern of gene expression that at least in part rely on posttranscriptional mechanisms. Several studies have suggested that all mRNAs required for germination and pollen tube growth are already present in the mature pollen grain and maintained in a translationally silent state until the progamic phase (Honys et al., 2000; Honys and Twell, 2004; Scarpin et al., 2017; Hafidh et al., 2018). Nonetheless, how male gene expression is posttranscriptionally regulated to permit correct pollen guidance is largely unknown, and the mRNA-regulating factors required for proper ovular guidance of pollen are currently unclear.

In the present study, we further explored the role of LARP6C and determined that it is a pollen-specific factor required for male fertility during the progamic phase. We provide evidence that the loss of LARP6C affects lipid synthesis and homeostasis as well as vesicular trafficking. Moreover, our experimental results support the notion that LARP6C orchestrates the balance between the translation, storage, and decay of its mRNA clients through direct binding, thus intervening in the guided growth of the pollen tube.

## Results

### LARP6C and its RNA-binding domain are required for male fertility at the pollen tube guidance step

Immunoblotting and high-throughput transcriptomic analyses (Klepikova et al., 2015) showed that, unlike LARP6A and 6B, LARP6C is almost exclusively expressed in pollen grains and pollen tubes (Figure 1A; Supplemental Figure S1). We therefore investigated its role in male fertility using two Arabidopsis T-DNA insertion mutants, *larp6c-3* and *larp6c-4*. Immunoblotting showed that both alleles are loss-of-function (lof) mutants (Figure 1B). To establish whether *larp6c* is a gametophytic mutation, we monitored the transmission efficiency (TE) through the female ( $TE^f$ ) and the male ( $TE^m$ ) gametophytes by reciprocal crosses with the wild-type (WT) and heterozygous *larp6c-3/+* or *larp6c-4/+* mutants (Figure 1C). Both alleles were transmitted normally through the female gametophyte ( $TE^f$  *6c-3* = 100% and *6c-4* = 96.7%), whereas their transmission through the male was significantly reduced, with *6c-3* showing  $TE^m$  = 74.1% and *6c-4*  $TE^m$  = 68.2% (Figure 1C). This suggests that male but not female fertility is compromised by the loss of LARP6C function.

There are different stages at which the male gametophyte could be deficient, including pollen development,

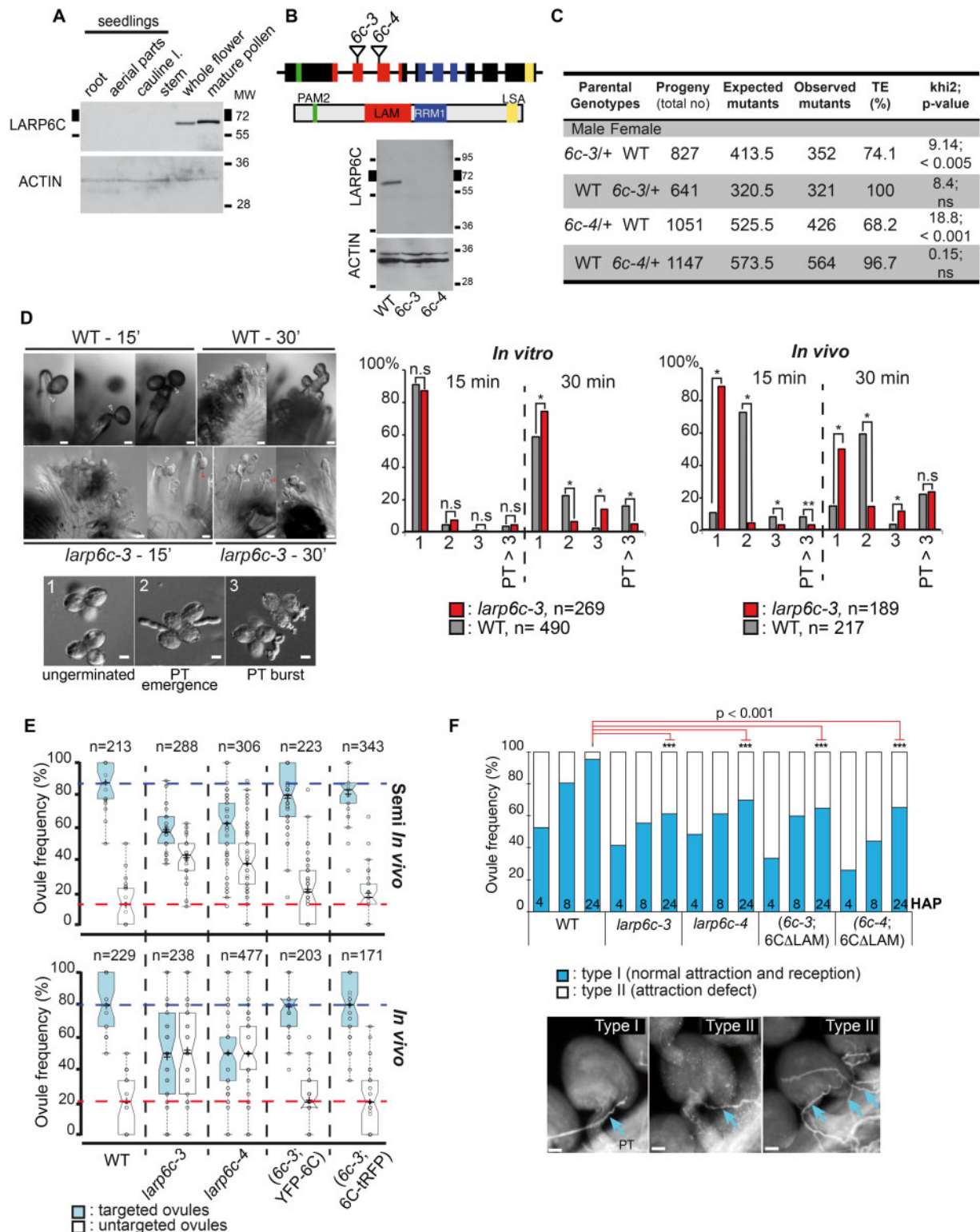


**Figure 1** LARP6C is required for pollen tube guidance. **A**, Immunoblot analysis of steady-state LARP6C protein accumulation. The same blot was probed with antibodies against LARP6C or ACTIN as a loading control. **B**, *larp6c-3* and *larp6c-4* alleles are *lof* mutants. Top panel: schematic representation of the *LARP6C* gene and *LARP6C* protein. Plain boxes represent exons and lines represent introns. The color code for exons is identical to that for the conserved protein domains. The insertion sites of the T-DNAs in *larp6c-3* and *6c-4* mutants are reported. Bottom panel: immunoblot analysis of *LARP6C* accumulation in flowers from the WT, *larp6c-3* and *6c-4* lines. ACTIN was used as a loading control. **C**, Transmission efficiencies of *larp6c-3* and *6c-4* mutant alleles. TE was calculated as:  $\left(\frac{\text{No. of mutant}}{\text{No. of WT}}\right) \times 100$ . ns: the number of mutant seedlings in the progeny is not significantly different from the expected number of mutant seedlings. **D**, Scoring of germination rate, pollen tube bursting, and elongation in vitro and in vivo. Left panels show representative images of in vivo (upper part) and in vitro (lower part) experiments. On the right,

germination, pollen tube growth or guidance, and sperm delivery (Johnson and Preuss, 2002). We monitored these pollen stages in *larp6c-3*, *6c-4*, and WT plants (Figure 1, D–F; Supplemental Figure S2, A–E). Assessment of male gametophyte maturation by DAPI staining revealed that 10% of the *6c-3* and *6c-4* mutant pollen grains did not complete their maturation and were arrested at the bicellular stage, compared to less than 3% in the WT (Supplemental Figure S2A).

We next monitored germination and pollen tube growth during the early and late steps after hydration (in vitro) or pollination (in vivo and semi in vivo [SIV]; Palanivelu and Preuss, (2006); and “Methods” section; Figure 1D; Supplemental Figure S2). In vitro, *larp6c-3* showed some defects in germination, with over 70% of ungerminated pollen grains after 30 min incubation versus 60% for the WT and an increased frequency of pollen tube burst. Moreover, at 30 min, *larp6c-3* showed less than 5% elongated pollen tubes versus 20% in the WT, for example, pollen tubes with lengths over three times that of mature pollen grains. In vivo, the situation appeared more dramatic, with a very high levels of ungerminated *larp6c-3* pollen at 15 and 30 min after pollination of over 80% and 50%, respectively, compared to the WT pollen, which showed less than 10% ungerminated pollen after 15 min incubation. Moreover, in vivo, at 30 min, *larp6c-3* pollen tubes seemed to be more prone to bursting than the WT (Figure 1D). These germination and pollen tube growth defects were likely due to delays rather than full arrest, since 7 and 24 h after pollination (HAP; Supplemental Figure S2, B, C, and E) or 4 h after hydration (Supplemental Figure S2D), the density and length of *larp6c* pollen tubes were similar to those of the WT.

We next investigated the requirement for LARP6C for pollen tube guidance and ovule targeting competence (Johnson and Preuss, 2002). We set up SIV experiments using pistils from *ms1* plants, a male-sterile mutant with normal pistil function (van der Veen and Wirtz, 1968), to assess the ability of *larp6c*-deficient pollen tubes to be guided through the pistil tissues towards the WT ovules for fertilization (Figure 1E, top panel; Supplemental Figure S3A). Whereas the WT pollen targeted 80% to 100% of the ovules (with a median value of around 90%), both *larp6c-3* and *6c-4* pollen showed a significant reduction, targeting 50%–70% of the WT ovules (with a median value of 60%). This failed pollen tube guidance phenotype was rescued by the N- and C-terminal

LARP6C fusion constructs (YFP-LARP6C and LARP6C-tRFP; Figure 1E; Supplemental Figure S3, B–C). In competition assays, irrespective of the order of pollination or the side of the stigma in which the pollen grains were dusted on, *larp6c-3* and *6c-4* pollen also showed a clear deficiency in ovule targeting, with a maximum targeting efficiency of 20% compared with the expected 50% rate (Supplemental Figure S3, A and D). This further supports the notion that the observed guidance phenotype directly relates to *larp6c* deficiency.

We next monitored the ability of the *larp6c* and *larp6c*-complemented pollen to target ovules in planta (Figure 1, E and F; Supplemental Figure S2E). We hand pollinated *ms1* pistils and following aniline blue staining, scored the number of targeted and nontargeted ovules. Aniline blue stains callose-like polysaccharides contained in pollen tube walls, and after exposure to UV emits yellow-green fluorescence that allows visualization of pollen tubes even after penetration in the ovule. Here, again the *larp6c* deficient pollen tubes displayed only 60% ovule targeting efficiency versus the 80% average observed in the WT pollinated pistils (Figure 1E, bottom panel). The targeting efficiency by the (*larp6c-3*; LARP6C-tRFP) and (*larp6c-3*; YFP-LARP6C) complemented lines recovered to a WT frequency (Figure 1E). Considering that 4 HAP, the density and length of mutant pollen tubes were similar to those of the WT (Supplemental Figure S2E), it appears unlikely that the ovule targeting deficiency of *larp6c* pollen was due to delays in germination or pollen tube elongation. Nonetheless, to completely rule out this possibility, we monitored the type of ovule targeting defects at 4, 8, and 24 HAP in vivo. We observed and scored two types of behavior: type I: if pollen tube attraction and reception were normal and type II: if pollen tube attraction was defective. We did not observe a situation where attraction was normal but reception defective. Consistent with previous experiments, we found that *larp6c*-deficient pollen tubes showed a significant increase in type II behavior compared to the WT (Figure 1F). At 24 HAP, while some 40% of the ovules remain unfertilized in pistils pollinated with *larp6c-3* or 4 mutant pollen due to attraction defects, only 5% of the ovules were not fertilized when pollination was conducted with the WT pollen (Figure 1F).

Considering that LARP6A mRNA is highly expressed in pollen (three to four times more than LARP6C mRNA in

graphs report the frequency of ungerminated pollen (1), PT emergence (2), PT burst (3), and PT longer than three lengths of the pollen grain (PT > 3) 15 or 30 min after pollination. *n* represents the number of scored pollen grains. E, SIV (upper panel) and in vivo (bottom panel) pollen tube guidance assays. For SIV assays, the WT ovules were arranged around homozygous *ms1* pistil explants pollinated with pollen from various homozygous backgrounds. For in vivo assays, homozygous *ms1* pistils were pollinated in planta with pollen from various homozygous genotypes. For each type of experiment, the numbers of targeted (blue boxes) and nontargeted (white boxes) ovules were scored and results represented as whisker notched boxplots. The genotypes of the pollen used for fertilization are recorded below the graphs and *n* is the total number of ovules scored in each experiment. The dotted lines respectively show the WT mean values of targeted (blue) and nontargeted (dark red) ovules by the WT pollen. F, In vivo scoring of pollen tube behaviors. The WT pistils were pollinated in planta with pollen from various homozygous genotypes (recorded below the graph) and the behavior of pollen tubes monitored and scored over a time course: 4, 8, and 24 HAP. Type I (blue bars): targeting and reception are normal, type II (white bars): attraction (targeting) is defective. Below the graph are representative images of the type of behaviors observed. Scale bars correspond to 10  $\mu$ m. The table below the graphs reports the numbers of scored ovules (*n*). *P*-values were calculated with an unpaired Student's *t* test. ns, not significant; \**P*  $\leq$  0.05, \*\**P*  $\leq$  0.01, \*\*\**P*  $\leq$  0.001.

mature pollen grain, [Supplemental Figure S1A](#)), we wondered whether LARP6A and LARP6C could at least partially act redundantly. In backcross experiments, *larp6a-1* lof pollen ([Supplemental Figure S3F](#)) displayed over 95% TE, and the TE of (*larp6c-3; larp6a-1*) was not significantly different from that of single *larp6c-3* mutant pollen (82.7%; [Supplemental Figure S3F](#)). We also ran in vivo pollination assays with the WT, *larp6c-3*, or (*larp6c-3; larp6a-1*) pollen and scored fertilization behaviors ([Supplemental Figure S3G](#)). Consistent with the results of backcross experiments, the absence of LARP6A did not affect fertilization in the WT or *larp6c* null background.

Finally, to confirm that *larp6c* lof specifically affects male fertility, we examined the capability of *larp6c-3* and *6c-4* mutant ovules to attract the WT pollen tubes by SIV and in vivo assays and found no significant difference from the WT ([Supplemental Figure S4](#)). A detailed description of these experiments can be found in the legend of [Supplemental Figure S4](#).

We previously demonstrated that LARP6C is an RBP and that its La-module is sufficient to bind RNA homopolymers in vitro ([Merret et al., 2013b](#)). We hence wondered whether the RNA-binding function of LARP6C is necessary for its role in pollen tube guidance. As for LARPs, including human LARP6, which carry a bipartite La-Module, the LAM is absolutely necessary to bind RNA both in vitro and in vivo ([Cai et al., 2010a](#); [Martino et al., 2015](#)), we constructed a truncated LARP6C deleted of its LAM (*LARP6C $\Delta$ -LAM*). We then stably expressed this deletion mutant construct in the *larp6c-3* and *larp6c-4* backgrounds under the control of the LARP6C native promoter ([Supplemental Figure S3C](#)). In vivo fertilization assays showed that pollen expressing *LARP6C $\Delta$ -LAM* had the same pollen tube guidance defects as *larp6c* lof pollen, suggesting that *LARP6C $\Delta$ -LAM* cannot complement the *larp6c-3* lof phenotype and that the La-Module RNA-binding motif is essential for LARP6C function in pollen tube guidance ([Figure 1F](#)).

In summary, our results support the notion that LARP6C is required for male fertility at least in part at the progamic phase through its function in pollen germination and during pollen tube guidance and does not appear to act redundantly with LARP6A. Moreover, LARP6C function in pollen tube guidance requires an intact La-Module, supporting the notion that this physiological role involves the RNA-binding activity of LARP6C.

### LARP6C forms dynamic cytoplasmic granules in mature pollen grains and in pollen tubes

To better understand the cellular roles of LARP6C, we monitored its subcellular distribution across pollen maturation and during pollen tube growth ([Figure 2A](#); [Supplemental Figure S5](#)). In microspores, LARP6C was only detected in the nucleolus. At the bicellular stage, LARP6C was much more generally distributed in the cytoplasm of the vegetative cell, as well as in the vegetative and generative cell nuclei. At the

tricellular stage, the subcellular distribution of LARP6C was similar to that at the bicellular stage, with possibly reduced amounts of LARP6C in the sperm cell nucleus compared to other subcellular compartments. In mature pollen grain, LARP6C displayed a complex localization pattern. It was clearly present in vegetative cell cytoplasm but transitioned from a diffuse pattern to a granular, aggregate-like pattern ([Figure 2A](#); [Supplemental Figure S5](#)). In addition to this granular distribution, LARP6C appeared to concentrate around the membrane surrounding the vegetative cell nucleus, the sperm cells and the cytoplasmic connection linking the sperm cell 1 to the vegetative cell nucleus.

To determine more precisely the distribution of LARP6C in mature pollen grains, we performed colocalization experiments between LARP6C-tRFP and various markers ([Figure 2B](#)). The histone H2B-GFP fusion protein, expressed under the control of the tomato (*Solanum lycopersicum*) pollen-specific *LAT52* promoter ([Twell et al., 1989](#)), was used to label the vegetative cell nucleus, thereby demonstrating the absence of LARP6C in this compartment. GEX2 is a sperm cell-expressed transmembrane protein ([Mori et al., 2014](#)) that labels the sperm cell membranes and the cytoplasmic connection between sperm cell 1 and the vegetative cell nucleus ([Brownfield et al., 2009](#); [McCue et al., 2011](#); [Mori et al., 2014](#)). Confocal analyses showed that LARP6C and GEX2 displayed distinct distributions ([Figure 2B](#)). The tRFP signal surrounded the GFP-GEX2 signal decorating the outer membrane of the male germ unit but not the membrane connecting the two sperm cells (the inner membrane), supporting the notion that LARP6C is excluded from the sperm cells and therefore only resides in the vegetative cell cytoplasm in mature pollen.

We next inquired on the nature of LARP6C cytoplasmic foci ([Figure 2B](#)). Eukaryotic cells contain many types of membrane-less cytoplasmic aggregates composed of translationally silent mRNAs and RBPs ([Buchan, 2014](#)). So far, only two types of mRNP granules have been identified in plant cells: processing bodies (p-bodies) and stress granules ([Weber et al., 2008](#)). Plant p-bodies are—as in other eukaryotes—characterized by the presence of actors of the general mRNA turnover process, such as the DCP1/DCP2 decapping holoenzyme, the XRN4 exoribonuclease, or the deadenylation complex. Stress granules, on the contrary, contain factors belonging to the translational machinery, including the PABP ([Weber et al., 2008](#)). First clues on the nature of LARP6C aggregates observed in mature pollen were derived by colocalization experiments with specific markers of p-bodies and stress granules, namely DCP1 and PABP, respectively. We used a YFP-tagged DCP1 protein expressed from its own upstream genomic sequences ([Merret et al., 2013a](#)). Although YFP-DCP1 displayed a punctuate distribution in the vegetative cell cytoplasm, similar to LARP6C, no obvious colocalization of DCP1 and LARP6C was observed. Of note, DCP1 accumulation appeared to be restricted to the vegetative cell cytoplasm, at least in mature pollen, and contrary to

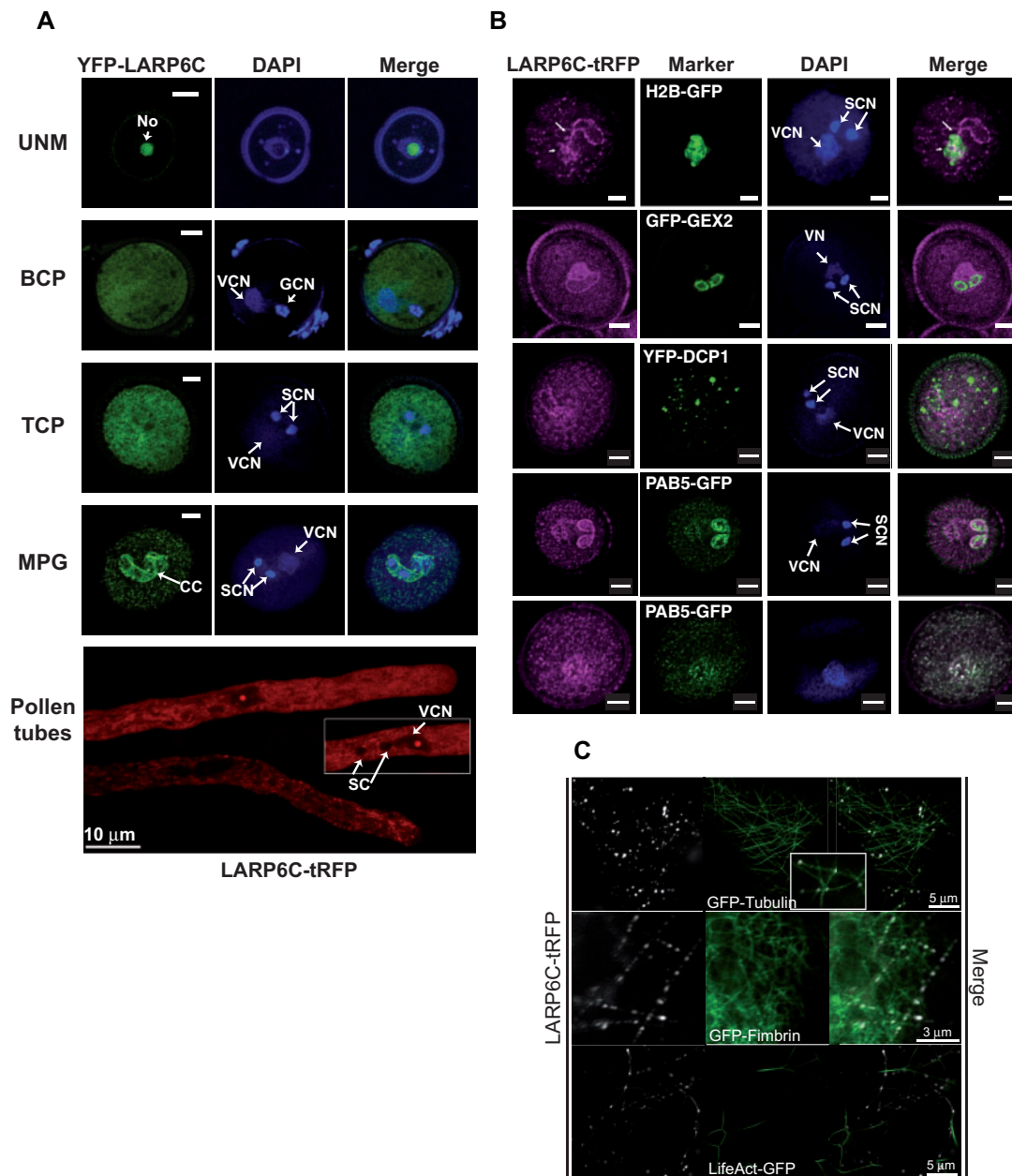


**Figure 2** Subcellular distribution of LARP6C across pollen development and pollen tubes. A, Subcellular localization of fluorescently tagged YFP-LARP6C by confocal microscopy at different stages of pollen maturation. UNM, uninucleate microspore; BCP, bicellular pollen; TCP, tricellular pollen; MPG, mature pollen grain and pollen tube. Scale bars correspond to 5  $\mu$ m for pollen and 10  $\mu$ m for pollen tube images. Representative images of LARP6C fused at its C-terminus with a tagRFP reporter are shown in Supplemental Figure S5A. B, Confocal observation of mature pollen grains that stably coexpress the LARP6C-tRFP fusion and the H2B-GFP fusion, the GFP-GEX2 fusion, the YFP-DCP1 fusion, or the PAB5-GFP fusion. Except for the H2B-GFP marker, which is expressed from the tomato *LAT52* promoter, all marker genes are expressed from their own upstream genomic sequences. Scale bars correspond to 5  $\mu$ m. In (A) and (B), arrows indicate the position of the nucleolus (No), generative cell nucleus (GCN), vegetative nucleus (VCN), sperm cell nucleus (SCN), and cytoplasmic connection (CC). C, Confocal observation of *N. benthamiana* epidermis cells transiently expressing the LARP6C-tRFP fusion coexpressed with microtubule-binding GFP-AtTUB6 and two actin-binding GFP-FABD2 or LifeAct-GFP reporters.  $n = 20$  cells from three independent infiltration repeats.

LARP6C, it did not localize at the periphery of the sperm cells or the vegetative nucleus (Figure 2B).

The Arabidopsis genome contains seven genes (*PAB2* to 8) encoding canonical PABPs, including *PAB3*, 5, 6, and 7 (Belostotsky and Meagher, 1996; Belostotsky, 2003; Honys and Twell, 2004), whose transcripts accumulation is

restricted to pollen. We fused the genomic sequence of the *PAB5* gene (the most highly expressed of the pollen specific *PABP* genes) to a YFP tag under the control of its own upstream sequences. In the vegetative cell cytoplasm, the YFP-PAB5 protein displayed a pattern identical to that of the LARP6C protein in that it accumulated in foci

surrounding the sperm cells and was excluded from the vegetative nucleus, but contrary to LARP6C, it was also present in the cytoplasm of sperm cells.

Finally, in pollen tubes, LARP6C was clearly excluded from the sperm cells and restricted to vegetative cell cytoplasm. In the cytoplasm, LARP6C signals showed various degrees of aggregate patterns, with foci appearing to be organized along a longitudinal string-like structure (Figure 2A; Supplemental Figure S5C). To explore the possibility that LARP6C foci could bind to the cytoskeleton structure, we coexpressed LARP6C-tRFP with GFP-AtTUB6 (which labels microtubules) in *Nicotiana benthamiana* epidermis cells (Ambrose and Cyr, 2007), GFP-FABD2 (Voigt et al., 2005), or LifeACT-GFP (Cvrčková and Oulehlová, 2017); which label actin microfilaments (Figure 2C; Supplemental Movie S1). While LARP6C did not significantly colocalize with actin microfilament markers, it colocalized with GFP-tubulin (Figure 2C; Supplemental Movie S1). Not only did the strings formed by LARP6C foci overlap with tubulin filaments, but LARP6C foci also appeared to move along microtubules, as revealed by time series observations (Supplemental Movie S1).

Finally, as an additional exploration of possible redundancy, we ran colocalization experiments between LARP6C and LARP6A (Supplemental Figure S5, B and C). We previously showed that, when transiently expressed in onion epidermis cells, LARP6C localized to stress granules (together with PABP), while LARP6A did not. Consistently, in mature pollen grain, we observed that LARP6C formed foci, while LARP6A did not (Supplemental Figure S5C). Additionally, LARP6A and 6C showed distinct subcellular distributions in pollen tubes, with 6A mainly accumulating in sperm cell cytoplasm while 6C was excluded from the sperm cells (Supplemental Figure S5C).

In summary, our data indicate that LARP6C shows a dynamic subcellular distribution across pollen maturation. We found that in mature pollen and pollen tubes, LARP6C is restricted to the vegetative cell cytoplasm and is present in aggregates that could possibly associate with microtubules.

### RIP-seq pulldown reveals LARP6C mRNA targets in mature pollen grain

The presence of LARP6C in cytoplasmic aggregates, which contain the PABP, together with our previously published data (Merret et al., 2013b), strongly support the notion that at the cellular level, LARP6C likely acts to control mRNA fate in pollen. In addition, since its RNA-binding domain is necessary to fulfill its role in pollen tube guidance, we reasoned that the identification of its mRNA clients would help reveal how LARP6C controls male fertilization at the molecular level. We hence sought to identify its mRNA targets using an unbiased RNA immunoprecipitation and sequencing (RIP-seq) strategy. We conducted the RIP procedure from complemented *larp6c-3* lof mature pollen grains expressing a PRO<sub>6C</sub>:LARP6C-FlagHA tagged version (6C-FH hereafter; Supplemental Figure S3, B and C) and from the WT pollen

grains as a negative control. After assessing the efficiency of the immunoprecipitation through immunoblotting (Supplemental Figure S6A), RNAs were extracted from the input and eluate fractions and subjected to RNA-seq. After mapping and filtering of the data set (see Supplemental Methods), a read per kilobase per million mapped reads (RPKM) value was calculated for each protein-coding gene. The replicates were found to be reproducible (Supplemental Figure S6B), enabling us to build a table with a mean normalized value per gene and filter out those with less than 1 RPKM value in one of the four samples (input or eluate from the WT or 6C-FH; Supplemental Data Set S1). Using such criteria, we retained a list of 7,356 expressed transcripts.

We first filtered out transcripts based on input fraction values, retaining mRNAs that are not differentially expressed (DE) and show a fold change between 6C-FH and WT < 1.2 in order to select for transcripts whose levels did not vary between control and 6C-FH inputs. Then, from this trimmed list, we selected mRNAs that are DE (False Discovery Rate: FDR 0.01) and accumulated to a higher extent in the eluate fraction of 6C-FH compared to the WT (Figure 3A). Next, we selected mRNAs that were enriched by the immunoprecipitation procedure, by selecting those with a RE<sub>6C-FH</sub> (RE is the eluate over input ratio) value > 1. To further increase stringency and reveal mRNAs that are most likely to be direct targets of LARP6C, we compared the RE<sub>WT</sub> to the RE<sub>6C-FH</sub> and, based on the repartition of the values (Supplemental Figure S6, C and D) selected transcripts with an (RE<sub>6C-FH</sub>/RE<sub>WT</sub>) value of 3 or more (Figure 3B). Through the above series of filters, we identified a high-confidence list of 115 genes encoding direct or indirect mRNA targets of LARP6C (Supplemental Data Set S1).

No gene ontology term was found to be significantly enriched amongst the 115 mRNAs identified as potential LARP6C targets. Nonetheless, a gene-to-gene analysis shows that the majority of LARP6C targets encode factors likely to be involved in polarized cell growth and male fertilization. This includes protein involved in endomembrane system trafficking and synthesis, signalling factors, and kinases (Samaj et al., 2006; Grebnev et al., 2017) and most strikingly proteins involved in lipid metabolism and homeostasis control (Ischebeck, 2016; Figure 3C; Supplemental Data Set S1). Also, we found that some LARP6C targets are known actors of pollen gametogenesis, pollen germination, pollen tube growth and guidance, or tip-polarized growth, such as the growth of roots or neurons (Supplemental Data Set S1).

### Loss of LARP6C affects lipid metabolism and the endomembrane system during pollen tube growth

In angiosperms, lipids are crucial for male fertilization. Pollen tube elongation depends on lipids synthesized and stored in pollen grain before desiccation or produced on the way from pistil to ovule (Ischebeck, 2016). Amongst the list of LARP6C targets are actors involved in fatty acid synthesis, di- and triacylglycerol (TAG) synthesis and homeostasis,



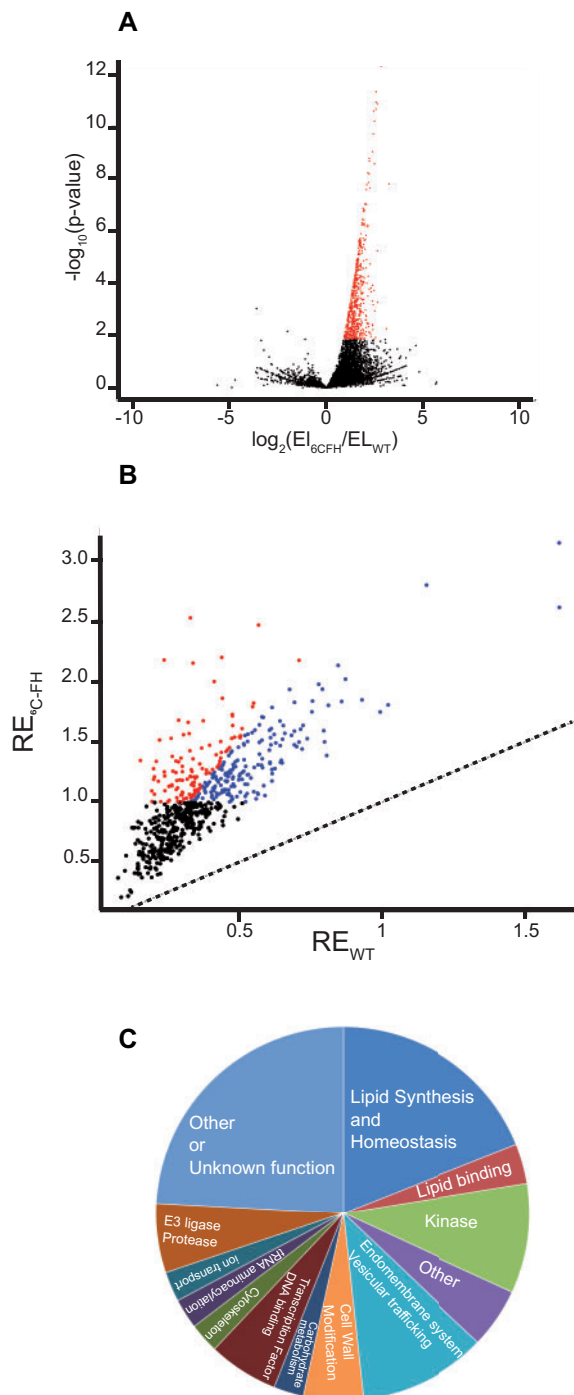


**Figure 3** RIP-Seq identification of LARP6C mRNA targets. **A**, Volcano plot repartition of the  $\log_2$  of fold changes between values in the eluate fractions of LARP6C-FH and WT for mRNAs found in the LARP6C-FH eluate fraction, according to their  $P$ -values obtained through the DESeq2 pipeline. Red dots represent mRNAs that are significantly more represented in LARP6C-FH eluates. A  $P \leq 0.01$  and  $FC \geq 1$  was used as significance criteria. **B**, Plotting the RE (Eluate-RPM/Input-RPM) values in LARP6C-FH against the RE values in the WT for the 635 mRNAs highlighted in graph A. mRNAs with a  $RE_{6C-FH} \geq 3RE_{WT}$  are labeled as blue dots. See [Supplemental Figure S6C](#) for a detailed description of the RIP-seq pipeline. **C**, Pie chart representation of the number of LARP6C targets within the various functional categories identified.

whose control were previously found to be necessary for correct pollen tube growth (Botté et al., 2011; Pleskot et al., 2012; Zheng et al., 2018). This includes genes encoding fatty acid synthesis factors (FAD2 (Botella et al., 2016), ACX4 (Khan et al., 2012), and AtLPEAT2 (Stålberg et al., 2009)); DGAT1, which catalyzes the first step of TAG synthesis (Zhang et al., 2009); DYRKP-2A (Schulz-Raffelt et al., 2016); and MPK6 kinases, which regulate TAG production (Zheng et al., 2018); SDP1, a TAG lipase involved in membrane lipid homeostasis control (Kelly et al., 2013); and MGD2, which catalyzes the synthesis of monogalactosyldiacylglycerol (MGDG; Botté et al., 2011).

Considering that LARP6C might control the expression of genes encoding proteins involved in glycerolipid metabolism and homeostasis at the posttranscriptional level, we tested lipid accumulation and synthesis in the absence of LARP6C in mature pollen grains and pollen tubes (Figure 4). First, we visualized lipid droplets (LDs), which consist of a phospholipid monolayer surrounding a core of neutral lipids, such as TAG and fatty acid steryl esters, by staining with Bodipy 505/515 (which stains neutral lipids) and Nile Red (which stains nonpolar and neutral lipids; Figure 4, A and B). In *larp6c-3* mature pollen grain, we did not detect any significant difference in staining compared to the WT grains (Figure 4A). We then germinated and grew WT and *larp6c-3* pollen tubes in vitro and visualized LD accumulation at 2 and 4 h post germination (Figure 4B). At 2 h after germination, 77 out 132 (58%) observed pollen tubes showed fewer LDs compared to the WT, and at 4 h, 84% ( $n = 100/119$ ) of pollen tubes showed an abnormal distribution of LDs. In 72% of the cases, LDs were absent from apical and subapical regions and were only detected in the shank, and 12% showed an overaccumulation and aggregation of lipids at the tip. Such aberrant distribution was never observed amongst the WT pollen tubes ( $n = 109$ ). This phenomenon was even more pronounced when pollen tubes were grown through a pistil explant, with 100% of *larp6c-3* pollen tubes showing an atypical distribution of LDs (Figure 4C, SIV). These results support the notion that lipid synthesis and/or distribution in pollen tubes is perturbed in the absence of LARP6C.

We next explored the impact of the downregulation of lipid synthesis on pollen tube guidance in the absence of LARP6C. Amongst the LARP6C mRNA targets, *MGD2* encodes a pollen specific (our data and Qin et al. (2009)) MGDG synthase (Botté et al., 2011). In situ labeling of Arabidopsis pollen tube membranes previously showed the presence of digalactosyldiacylglycerol (DGDG, which are synthesized from MGDG), and the chemical inhibition of the MGD enzymatic pathway with galvestine-1 reduces MGDG content and downregulates pollen tube elongation rates (Botté et al., 2011), supporting a role for MGD in male fertilization.

We reasoned that if one of the molecular bases of the guidance defect of *larp6c* relates to the misregulation of *MGD2* mRNA fate and expression, the specific inhibition of its enzymatic activity and downregulation of MGDG/DGDG

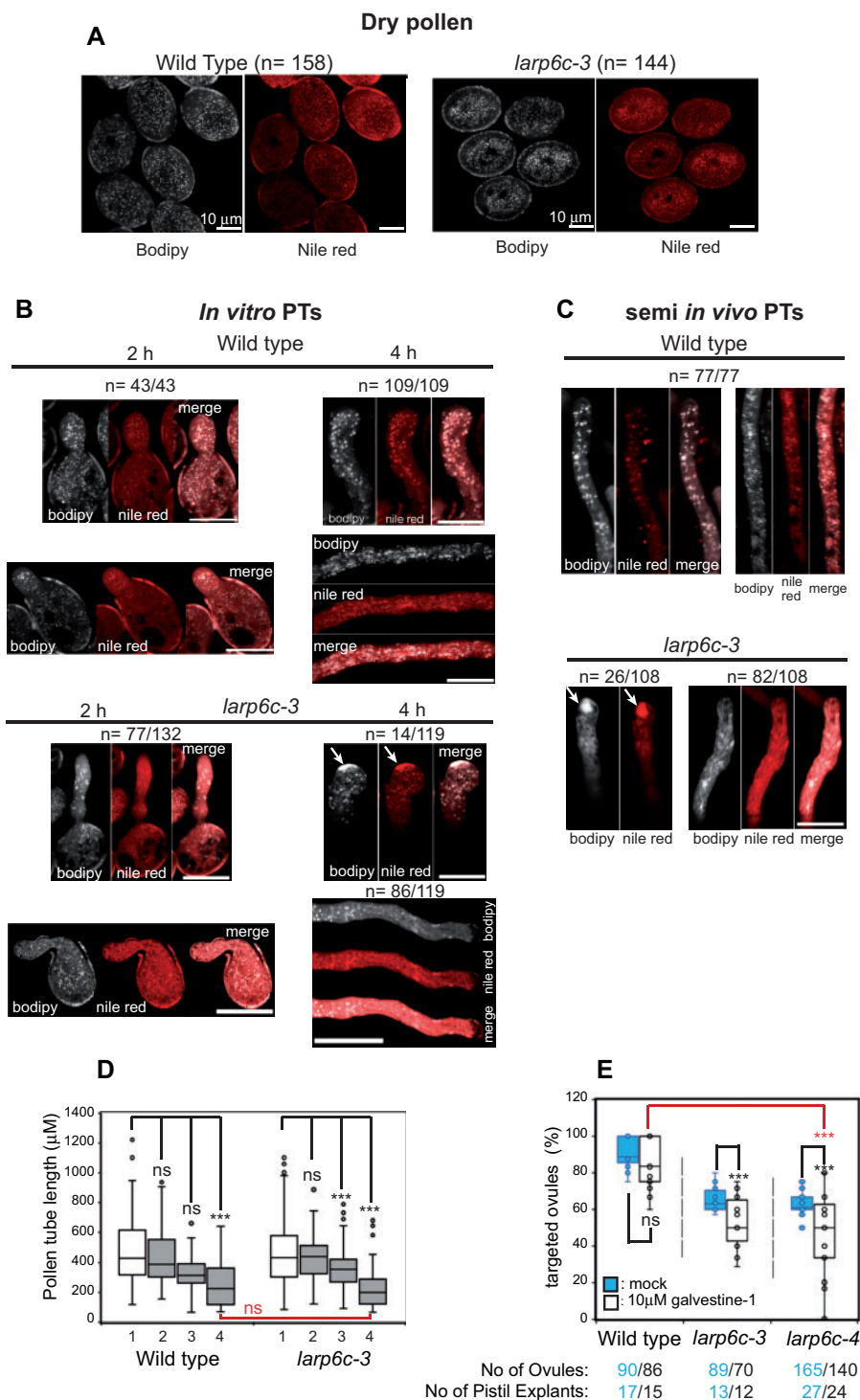


**Figure 4** The loss of LARP6C function affects lipid homeostasis in pollen tubes. The WT and *larp6c-3* pollen grains were stained with Bodipy 505/515 and Nile red at the mature pollen stage (MPG; A) or in pollen tubes (PTs; B and C). In (B) PTs were germinated and grown in vitro. PTs were collected at 2 h and 4 h after activation for staining. Representative images are shown. In (C) PTs grown SIV were collected 7 h following pollination (4 hap, pistils are cut at shoulder, placed on plate with ovules, and further incubated 3 h before scoring). *n* represents the number of pollen tubes with LDs distributed as on the presented image over the total number of observed pollen grains. Scale bars correspond to 10  $\mu\text{m}$  in (A) and to 5  $\mu\text{m}$  in (B, C). D, Monitoring of pollen tube growth in the presence of galvestine-1. Whisker boxplot representation of the length of the WT or *larp6c-3* pollen tubes grown in vitro for 4 h in the presence or absence of galvestine-1. 1: untreated, 2: mock (1% DMSO), 3 and 4: 5  $\mu\text{M}$  and 10  $\mu\text{M}$  galvestine-1. E, SIV pollen tube guidance assays. Assays were conducted either in the presence of 1% DMSO (untreated) or in the presence of 10  $\mu\text{M}$  of galvestine-1. Results are represented as whisker boxplots. *P*-values were obtained through an unpaired Student's *t* test; ns, not significant; \*\*\**P*  $\leq$  0.001.

production with galvestine-1 should alleviate or aggravate the *larp6c* lof phenotype. We hence monitored pollen tube elongation rates and pollen tube guidance in the presence of galvestine-1 by SIV assays (Figure 4, D and E). Consistent with a previous report (Botté et al., 2011), we observed that galvestine-1 application reduced pollen tube elongation in the WT pollen as well as *larp6c-3* mutant pollen (Figure 4D). However, when we monitored pollen tube guidance efficiency, the WT pollen tubes were only slightly or not affected at all, whereas pollen tubes of *larp6c* mutants showed a considerable decrease in ovule targeting in the presence of galvestine-1 (Figure 4E). Under these conditions, only 30%–60% of ovules were targeted by *larp6c*-pollen tubes, whereas the mock-treated samples showed 60%–70% targeting. In some pistil explants, *larp6c* pollen tubes showed no ovule targeting at all in the presence of the MGD inhibitor, a situation that was never observed with *larp6c-3* pollen tubes in the absence of the MGD inhibitor (Figures 1, E and F; 4E). Collectively, these results support a synergic effect between the lof of LARP6C and the pharmacological inhibition of MGD2 synthase activity on pollen tube guidance but not on pollen tube elongation.

LARP6C also binds mRNA encoding factors involved in endosome functioning and vesicular trafficking. Brefeldin A (BFA) is a fungal toxin known to perturb endomembrane system trafficking, particularly at the level of retrograde

Golgi to ER trafficking and to induce ectopic ER–Golgi fusions known as BFA bodies (Tse et al., 2006). We therefore monitored *larp6c-3* pollen tube sensitivity to BFA compared to the WT (Figure 5). After 1 h activation on germination medium, the pollen tubes were exposed to BFA and the number and size of BFA bodies scored over time through FM 4-64 staining. As soon as 10 min after exposure to BFA, *6c-3* pollen tubes showed increased number of BFA bodies and a dramatic increase in size compared to the WT 17 min after treatment. At this time point, ectopic BFA-particles were also bigger in the mutant than in the WT. These results indicate that pollen tubes deprived of LARP6C are hypersensitive to pharmacological perturbation of endosomal trafficking.

### LARP6C directly binds to the 5'-UTRs of its mRNA targets

We next sought to understand how LARP6C recognizes and influences the fate of its mRNA targets through binding. RBPs often bind to primary sequence motifs shared between their mRNA targets to regulate their fate. Considering that cis regulatory elements are mostly located in the 5'- and/or 3'-UTRs of transcripts, we looked for primary sequence motif(s) shared between the UTRs of the putative LARP6C targets. Using the Araport database, we found and retrieved the 5'- and 3'-UTRs for 112 mRNAs and ran a discriminative motif search using a MEME search (at the MEME suite portal (<https://meme-suite.org/>)). Whereas no significant motif could be detected in the 3'-UTRs of LARP6C mRNA targets, we identified two regions we named A-box ( $E^{\text{value}}$ :  $5.5E^{-99}$ ) and B-box ( $E^{\text{value}}$ :  $9.3E^{-91}$ ) motifs that are highly enriched in the 5'-UTRs of LARP6C mRNA targets (Figure 6A). As a control, we ran an identical motif search using a set of 112 randomly chosen 5'- and 3'-UTRs from genes expressed in pollen according to our transcriptomic analyses. We found no significant enrichment for an A- or a B-type region, supporting the idea that these sequence motifs are specific for mRNAs that are in a complex with LARP6C.

The A motif is a purine-rich 21 nt sequence with a clear dominance of A over G nucleotides, while the B motif is a pyrimidine-rich 21 nt sequence with a majority of U (T in DNA) over C repeats (Figure 6A; Supplemental Data Set S1). A closer examination of sequences that contain the A and/or B consensus sequence revealed two major categories for each box type. In particular, sequences harboring the A motif are mainly composed of either A or AG/AAG repeats, whilst sequences sharing the B consensus motif contain either U or UC/UUC repeats (Supplemental Data Set S1). Amongst the 112 identified 5'-UTRs, 70 (62.5%) bear the A motif, 74 (66%) the B motif, and 49 (43.7%) carry both (Supplemental Figure S6E).

The presence of motifs shared by transcripts that coimmunoprecipitated with LARP6C in vivo suggests that one or both of these boxes mediate the direct binding of LARP6C. To explore this hypothesis, we tested the RNA-binding unit of LARP6C, the La-module, for its ability to interact with

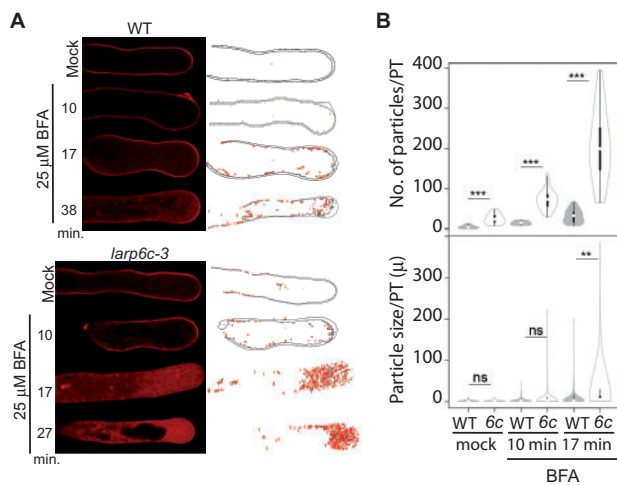


**Figure 5** Pollen tubes deprived of LARP6C are hypersensitive to BFA. Pollen grains were germinated in vitro and after 1 h activation on germination medium, pollen tubes were incubated with mock (DMSO) or 25-μM BFA. A, Representative images of FM4-64 staining captured at the respective times of the WT and *larp6c-3* PTs treated with mock or BFA. Sketched outline of the PTs with red dots (counts) describing the appearance of the particle frequency and size, as detected by the ImageJ particle analysis plug in. B, Following FM 4-64 staining, the number (top panel) and size (bottom panel) of BFA bodies was scored over a time course and represented as violin plots. Number of PTs observed to score particle number: WT: mock: 23, 10 min: 14, 17 min: 30; *larp6c-3*: mock: 32, 10 min: 35, 17 min: 25. Number of PTs observed to score particle size: WT: mock: 59, 10 min: 62, 17 min: 95; *larp6c-3*: mock: 61, 10 min: 115, 17 min: 189. P-values were obtained with an unpaired Student's *t* test. ns, not significant; \*\*P ≤ 0.01, \*\*\*P ≤ 0.001.

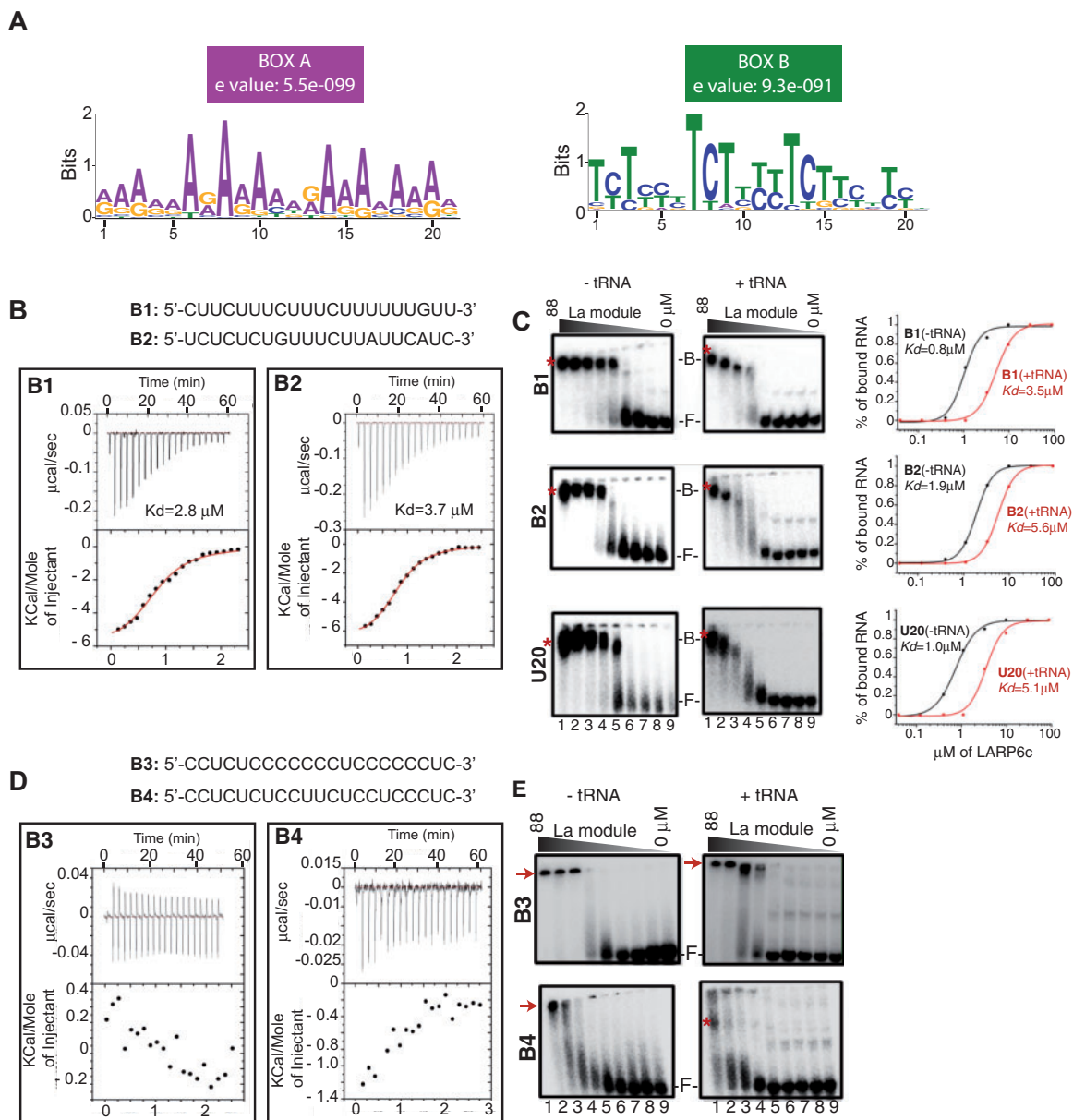


**Figure 6** The LARP6C La-module binds to B-type RNA boxes. **A**, Consensus sequences of the conserved motifs within the 5'-UTRs of LARP6C-bound mRNAs. Calorimetric (**B**, **D**) and EMSA (**C**, **E**) analyses of the interaction between the LARP6C La-module (encompassing residues 137–332) and oligos B1, B2 (**B**, **C**), U<sub>20</sub> (**C**), B3 and B4 (**D**, **E**). In (**B**) and (**D**) for each graph, the upper panel corresponds to the raw titration data showing the thermal effect of injecting an RNA oligo solution into a calorimetric cell containing the recombinant LARP6C La-module. The lower panels show the normalized heat per injection values obtained by integrating the raw data and subtracting the heat value of the RNA dilution. The red lines in the graphs for oligos B1 and B2 (**B**) represent the best fit derived by a nonlinear best-square procedure based on an independent binding site model. The dissociation constants (Kd) are indicated for the B1 and B2 oligos; the thermodynamic parameters are shown in [Supplemental Table S1](#). **C**, **E**, EMSAs of LARP6C La-module binding to: B1, B2 or oligo U<sub>20</sub> (**C**), B3 or B4 (**E**). Decreasing concentrations ( $\mu$ M; 88 [lane 1], 29.3 [lane 2], 9.8 [lane 3], 3.3 [lane 4], 1.1 [lane 5], 0.4 [lane 6], 0.12 [lane 7], 0.04 [lane 8], and 0 [lane 9]) of the recombinant LARP6C La-module were mixed with 3 nM of 5'-labeled oligos. B stands for Bound, F for Free, red asterisks mark the RNA-protein complex, and the red arrows on (**E**) shows samples retained into the gel wells. Experiments were conducted in the absence (-tRNA) or presence (+tRNA) of unlabeled competitor (tRNA<sub>mix</sub> of *E. coli* MRE 600 at 0.01 mg·mL<sup>-1</sup> concentration). Graphs in (**C**) show the quantification of the bound RNA fraction versus the protein concentration in the absence (black lines) or presence (red lines) of tRNA competitor. The values of the dissociation constants are reported. Kd values reported for the EMSA experiments were calculated out of three independent replicates with the following standard deviations: LARP6C-B1 (-tRNA): 0.8  $\pm$  0.1; LARP6C-B1 (+tRNA): 3.5  $\pm$  0.3; LARP6C-B2 (-tRNA): 1.9  $\pm$  0.3; LARP6C-B2 (+tRNA): 5.6  $\pm$  0.2.

these boxes in vitro ([Figure 6, B–E](#); [Supplemental Figure S7](#)). We designed two oligonucleotide sequences for the A motifs called A1 and A2, representing the “A-rich” and the “AG/

AAG-rich” types, respectively ([Supplemental Figure S7A](#)). Analogously, B1 and B2 were designed for the B motifs exemplifying the “U-rich” and “UC/UUC-rich” types,

respectively (Figure 6B). As a control, we designed oligos B3 and B4, representing C- or CU/CCU-rich sequences, respectively. A recombinant version of the LARP6C La-module, identical to the one used in Merret et al. (2013b), was expressed in *E. coli* as previously described and its ability to bind the A- and B-type oligo RNAs was quantified by isothermal titration calorimetry (ITC) and electrophoretic mobility shift assay (EMSA; Figure 6, B–E; Supplemental Figure S7). In the ITC experiments, serial titration of LARP6C La-module with RNA oligos B1 and B2 generated (in both cases) a profile that could be fitted to a sigmoid-shaped binding curve centered around a 1:1 stoichiometry, with a dissociation constant in the low micromolar range (Kds of 2.8 and 3.7  $\mu\text{M}$ , respectively, indicating direct binding of LARP6C La-module to B1- and B2-type motifs (Figure 6B; Supplemental Table S1). The binding mode of LARP6C La-module for the B1 and B2 oligos is similar (but with higher affinity) to that previously observed for an U20 homopolymer (Supplemental Table S1; Merret et al. (2013b)). On the contrary, no binding of oligos B3, B4, A1, or A2 to the recombinant LARP6C domain was detected by ITC under the same experimental conditions (Figure 6D; Supplemental Figure S7A; Table S1).

To confirm the ITC results, parallel EMSAs were performed using RNA oligos labeled at the 5' end with  $\gamma$ - $^{32}\text{P}$  to monitor RNA-protein complex formation by native gel electrophoresis. Experiments were conducted in the presence or absence of tRNA competitor. For oligos showing the ability to form a complex with La-module, the fraction of bound RNA was plotted against the protein concentration and the dissociation constant determined (Figure 6C). In agreement with the ITC results, EMSA confirmed that B1 and B2 oligos associate with the LARP6C La-module, with estimated dissociation constants in the low micromolar range (Kds of 0.8 and 1.9  $\mu\text{M}$ , respectively), again suggesting a high affinity of LARP6C La-module towards B1 and B2 oligos (Figure 6C). The binding behavior of B2 oligo was very similar to what we observed for an oligo(U<sub>20</sub>; Merret et al., 2013b), whereas B1 showed a slightly higher binding affinity. Assays with oligos A1, A2, B3, oligo(C<sub>20</sub>) and to a lesser extent with B4 were hindered by samples being retained in the wells of the gel at high protein concentration (Figure 6E; Supplemental Figure S7B), an issue most likely linked to protein and/or protein/RNA nonspecific aggregation (Hellman and Fried, 2007). Despite changing various experimental conditions, this issue could not be overcome. The presence of a tRNA competitor marginally helped in the case of B4, albeit association with LARP6C was observable only at high protein concentrations and a Kd could not be calculated, as the binding curve did not reach a plateau (Figure 6E).

Collectively, these experiments demonstrate that LARP6C La-module binds to oligos B1 and B2 with high affinity and with a similar association mechanism observed with oligo(U<sub>20</sub>). B1, which contains three stretches of U residues, one of which is six uridines long, appeared to bind slightly

more tightly than B2 and U<sub>20</sub>. Altogether, these results indicate that the LARP6C La-module strongly binds to B-type motifs and does not associate with A-type motifs, at least in vitro, and that it displays low affinity for B4.

We hence propose that in vivo, LARP6C directly binds (at least) to mRNAs that carry a B1- or B2-type box in their 5'-UTRs to execute posttranscriptional regulation on its mRNA targets.

### LARP6C is not required for the accumulation of its mRNA targets in mature pollen grain

To gain a global view of the role of LARP6C in the accumulation of its mRNA targets, we monitored the polyadenylated transcriptome of mature pollen grains in the absence of LARP6C. Pollen grains were collected from the WT and *larp6c-3* plants grown together in a greenhouse (see "Supplemental methods"), total RNAs were extracted from the pollen, and the polyadenylated fraction was subjected to next generation sequencing. Following mapping and filtering of the reads (see "Supplemental methods"), we retained a list of 7,399 transcripts with at least 1 RPKM as reliably expressed from both Col-0 and *larp6c-3* (Supplemental Figure S8 and Supplemental Data Set S2). We then used a DE-seq pipeline (FDR 0.05) to find genes whose transcripts differentially accumulate in the mutant background and retained those with a fold change of at least 1.5 between the WT and *larp6c-3*. We found 2,174 genes that were upregulated or downregulated in *larp6c-3* pollen compared to the WT (Figure 7A). Monitoring the fold changes of these transcripts between the WT and (*larp6c-3*; 6C-FH) in the input fraction of the RIP-seq samples, we observed that they are centered around 1 (Figure 7B). This suggests that the expression of the LARP6C-FlagHA transgene in the *larp6c-3* background fully complemented the *larp6c-3* mutation and restored a WT expression level, demonstrating that the LARP6C-FlagHA translational fusion is functional and that the misregulation of the *larp6c-3* pollen transcriptome is biologically significant and a direct consequence of the loss of LARP6C function. We then asked if the steady-state levels of LARP6C-bound mRNAs are affected in *larp6c-3* pollen grains. Of the 115 targets, 96 were detected in the RNA-seq data, and only 15 of these differentially accumulated in the *larp6c-3* background (Figure 7C; Supplemental Data Set S2). Of these, 10 were downregulated by 1.5- to 2.8-fold and five were upregulated by 1.5- to 1.7-folds in *larp6c-3* (Figure 7D). These observations suggest that, at least in dry pollen, LARP6C is not required for maintaining steady-state levels of its mRNA targets.

### LARP6C controls the expression of a reporter transcript containing a functional 5'-UTR B-box motif

To gain a mechanistic insight into the impact of LARP6C binding to its mRNA targets, we performed transient assays to monitor the expression of a *YFP* reporter gene under the

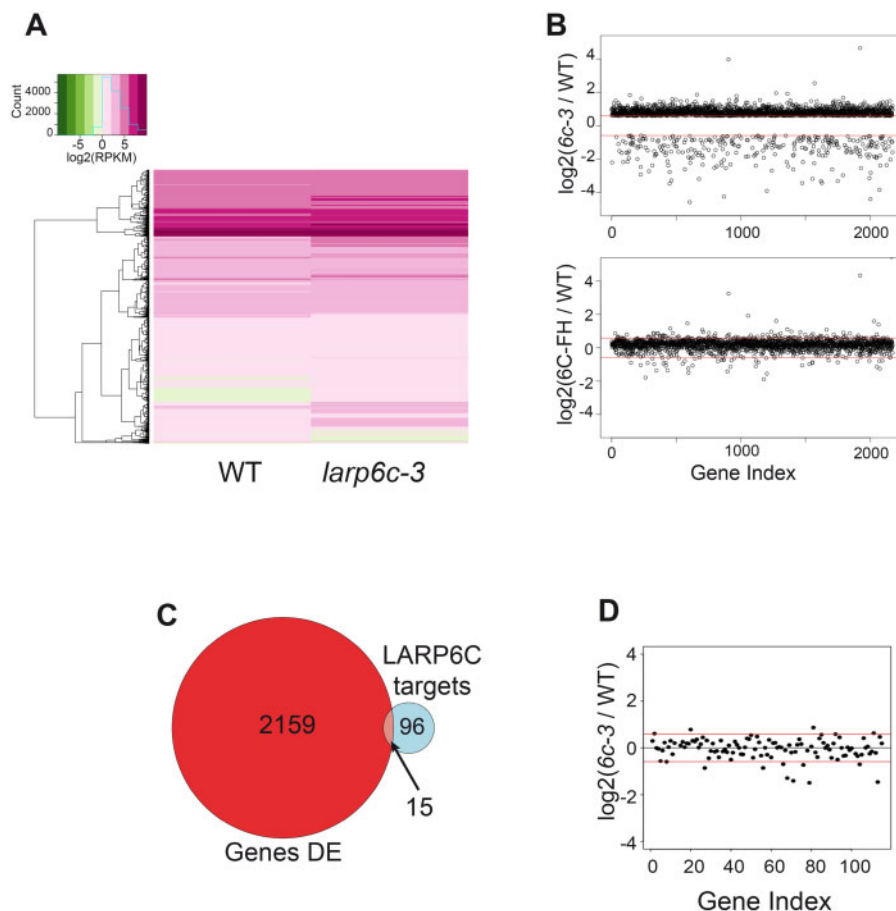


**Figure 7** *larp6c* lof does not affect the steady-state transcript levels of its target in dry pollen. **A**, Heat map representation of the log<sub>2</sub>(RPKM) values of genes that are DE between the WT and *larp6c-3* plants. The heat map was built from the list of DE genes with log<sub>2</sub>(RPKM) values between  $-2$  and  $+10$  (2,142 genes; 98.5% of the DE genes). **B**, Plot representation of the log<sub>2</sub> values of the ratios: (*larp6c-3*/WT; upper panel) and log<sub>2</sub>(6C-FH/WT; lower panel) for the 2,174 genes found to be DE in *larp6c-3* mutant pollen. Red lines mark the cut off value (log<sub>2</sub>(1.5) and log<sub>2</sub>(1/1.5)). **C**, Venn diagram representation of the number of transcripts that are DE in *larp6c-3* and/or immunoprecipitated by 6C-FH. Note that of the 115 RIP targets, 19 were not present in the transcriptomic data from RNA-seq. **D**, plot representation of the log<sub>2</sub>(*larp6c-3*/WT) for mRNAs identified by RIP-seq. Red lines mark the cut off value (log<sub>2</sub>(1.5) and log<sub>2</sub>(1/1.5)).

control of a modified 5'-UTR belonging to *MGD2*, a LARP6C mRNA target that carries a potential bona fide B-box and no A-box motif (Supplemental Data Set S1). We then respectively replaced the native B-box by two sequences that we demonstrated in vitro are strongly bound (B1-box) or not bound at all (B3-box) by the LARP6C La-module (Figure 6). We inserted the modified 5'-UTR sequences downstream of the CaMV35S promoter and fused to coding sequence of YFP (*B1-YFP* and *B3-YFP*) in a plant binary vector (Figure 8A). These YFP-containing plasmids were transiently expressed in *N. benthamiana* leaves individually or coinfiltrated with a plant binary vector expressing a tRFP-tagged LARP6C also under the control of the CaMV35S promoter. Three days post infiltration, leaves were collected and YFP mRNA and protein levels assessed (Figure 8, B and C). Quantitative analyses showed that when the LARP6C protein was present, *B1-YFP* transcript levels increased by two-fold (Figure 8B). Conversely, the coexpression of LARP6C with the *B3-YFP* construct did not significantly affect *B3-YFP* mRNA levels (Figure 8B). Remarkably, the

presence of LARP6C significantly reduced YFP protein accumulation when expressed from the B1 but not the B3 construct (Figure 8C). We also monitored the subcellular distribution of the tRFP-LARP6C fusion protein following agroinfiltration. Similar to findings for mature pollen grains (Figure 2) and onion epidermis cells following stress exposure, LARP6C formed foci in the cytoplasm of *N. benthamiana* leaves (Figure 8D). As in pollen grains and onion epidermis cells, LARP6C foci contained the PABP, we reason that LARP6C also likely aggregates into mRNP granules in *N. benthamiana*.

### LARP6C controls native *MGD2* protein levels and distribution in pollen tubes

We next asked whether LARP6C controls the mRNA and proteins levels of their target genes using *MGD2* mRNA as an example. We cloned the *MGD2* genomic locus (starting at position  $-579$  from ATG) including its native B-box motif in fusion with the YFP coding region that we placed at the C-terminus and transformed this chimeric gene into the

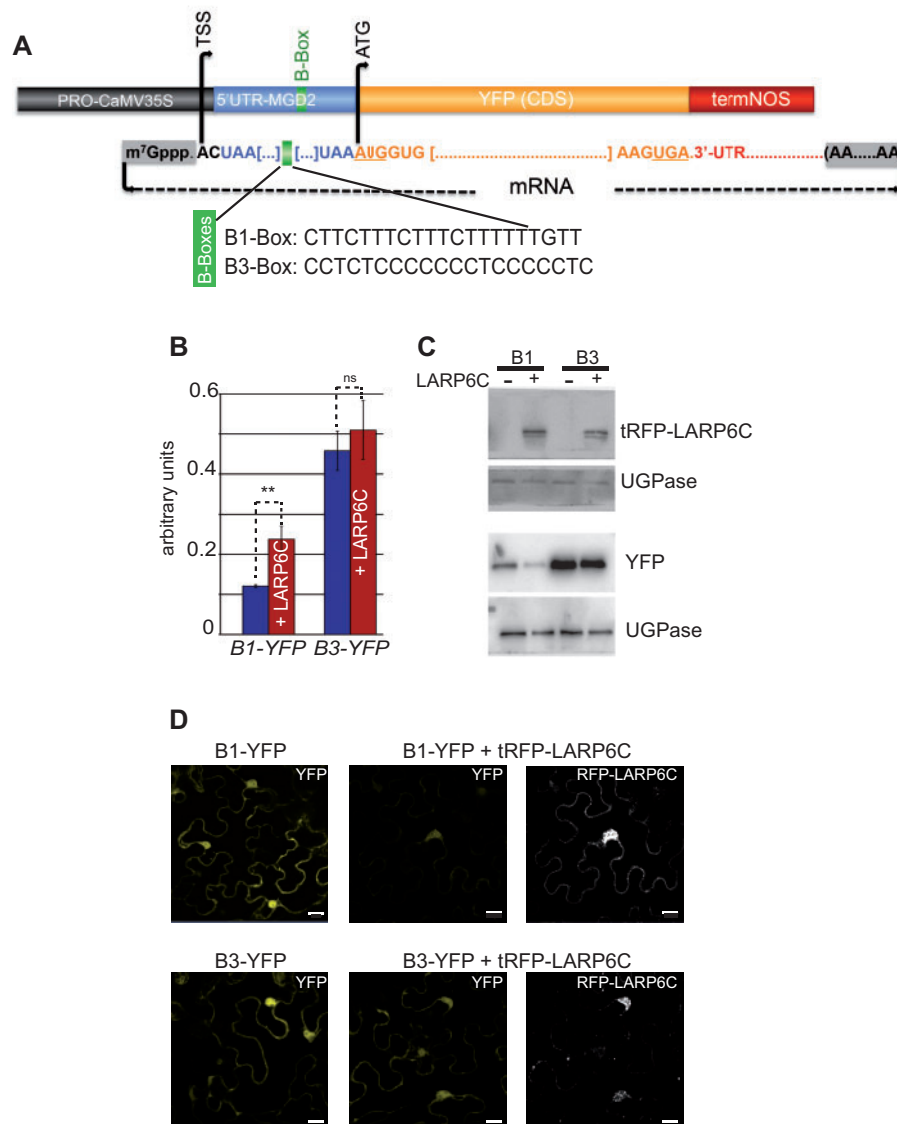


**Figure 8** LARP6C binding at the 5'-UTR of a reporter construct reduces protein and increases mRNA levels. A, Schematic representation of the YFP reporter constructs, B, RT-qPCR monitoring of YFP mRNA levels. To normalize YFP mRNA levels to transformation efficiency, we used the levels of *HPTII* mRNA encoded by the *HPTII* gene carried by the YFP binary plasmid but not the tRFP-LARP6C one. SDS were calculated from three biological replicates. *P*-value was obtained using a Student's *t* test. **\*\****P* < 0.005; ns, not significant. C, Immunoblot analysis of tRFP-LARP6C and YFP protein levels. Two immunoblots were prepared and respectively hybridized with anti-LARP6C or GFP antibodies. Levels of UGPase were used as the loading control. Representative images of three replicates are shown. D, Confocal imaging of YFP from leaves not transformed with tRFP-LARP6C (left panels) and of YFP and tRFP-LARP6C distribution (right panels). Scale bars represent 20  $\mu$ m. Leaves that were observed are different from those used to prepare total RNA and protein extracts. Representative images of three biological replicates are shown

WT background. We then screened pollen and pollen tubes from 22 primary transformants and selected line 6, which we crossed to *larpc6-3* homozygous plants. In the F2 generation, we selected plant homozygous for the *larpc6-3* allele that expressed heterozygous *MGD2-YFP*. We then performed microscopic observations of the WT and *larpc6-3* pollen that was heterozygous for the *MGD2-YFP* transgene. Pollen grains were placed on in vitro pollen germination agarose pad medium and YFP signals monitored in mature pollen grain (dry pollen), pollen at 15 and 30 min after hydration (Figure 9A), and pollen tubes at the 4 h time point

(Figure 9B). Strikingly, both in the WT and *larpc6-3*, mature pollen grains show very low levels of YFP signal, which intensified over time upon hydration and in pollen tubes.

To confirm this finding and to assess the role of LARP6C in MGD2 protein accumulation, we quantified fluorescence intensity in dry pollen and at 1 and 4 h after activation. As shown in Figure 9C, MGD2-YFP levels drastically increased in pollen tubes 1 h after activation in both the WT and mutant. Nonetheless, compared to the WT, *larpc6-3* dry pollen showed higher levels of fluorescence, a situation opposite that observed in 1 h pollen tubes, which showed reduced

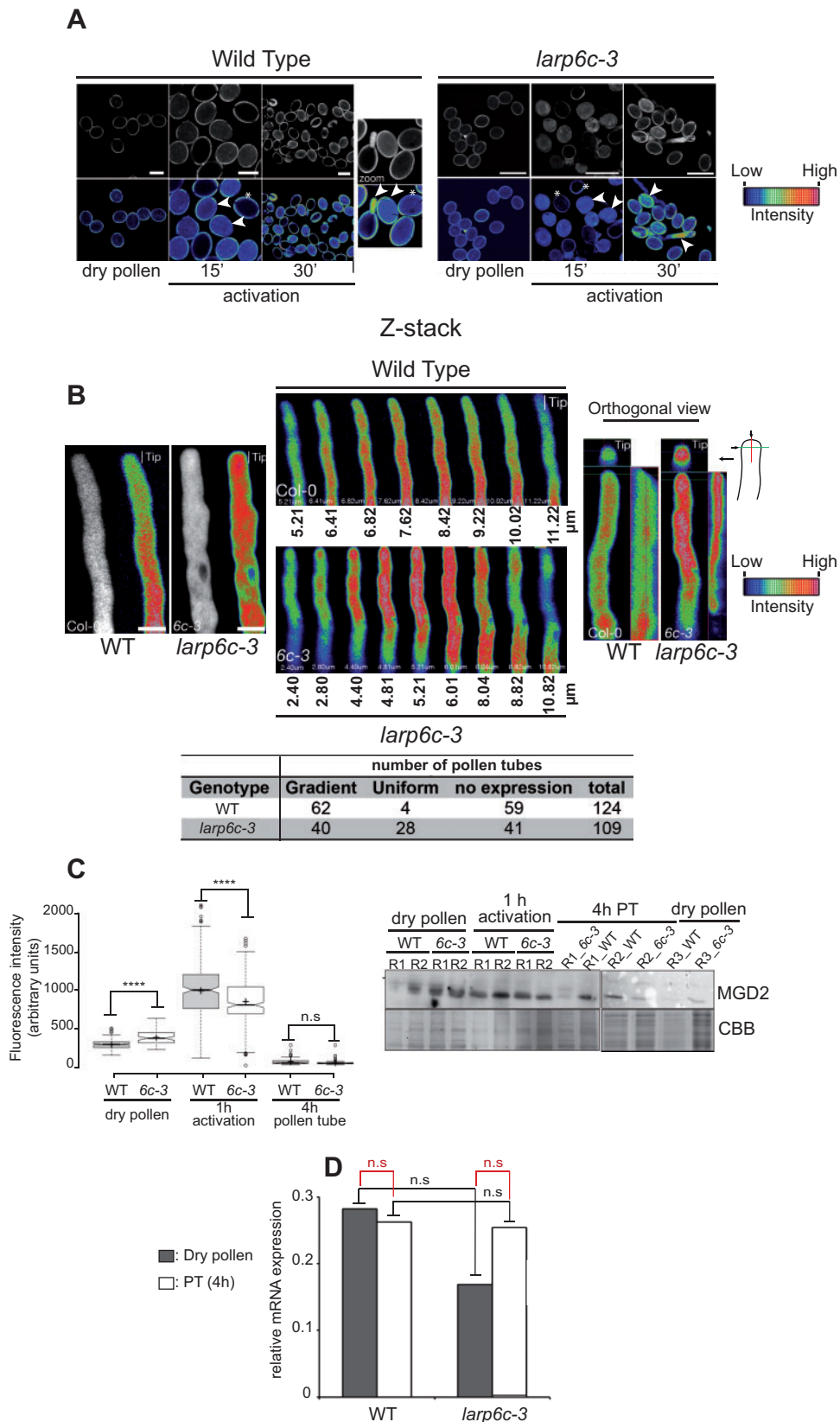


**Figure 9** LARP6C is involved in the dynamic fine-tuning of MGD2 protein accumulation in vivo. Monitoring of the levels of MGD2-YFP fusion protein expressed from the *MGD2* native promoter (*PRO<sub>MGD2</sub>:MGD2-YFP*) and endogenous MGD2 in the WT and *larp6c-3* plants. **A**, Representative images of YFP signal in heterozygous mature pollen grains at activation: 0, 15, and 30 min after incubation on in vitro germination medium. Bottom panels show images in pseudo color with the associated scale bar representing the intensity of the YFP signal. White arrows and asterisks respectively point to segregation pollen grains expressing or not expressing the translational fusion. **B**, Live cell imaging of MGD2-YFP



MGD2-YFP signals in the absence of LARP6C. Using specific antibodies (Awai et al., 2001), we made similar observations for endogenous MGD2 accumulation, finding significantly more protein in pollen tubes than in dry pollen. Moreover, the loss of LARP6C function induced the overaccumulation of MGD2 in mature pollen and underaccumulation in pollen tubes compared to the WT (Figure 9C, right panel). Next, quantitative reverse transcription polymerase chain reaction (RT-qPCR) assays revealed that the mRNA levels of MGD2-YFP and endogenous MGD2 did not significantly vary before and after pollen hydration and that the loss of LARP6C did not affect mRNA levels (Figure 9D). This is consistent with previously published transcriptomic data showing that endogenous MGD2 mRNA levels did not significantly vary between dry pollen and pollen tubes after 30 min or at 4 h activation in vitro (Qin et al., 2009).

Beyond an impact on protein levels, the loss of LARP6C function also appeared to affect MGD2-YFP distribution along the pollen tube (Figure 9B). In the WT, MGD2-YFP signal showed a diffuse cytosolic pattern, with the signal intensity distributed along a gradient decreasing from the shank toward the tip in almost 94% ( $n = 124$ ) of the pollen tubes. In the absence of LARP6C, the gradient distribution of MGD2-YFP was lost in 59% ( $n = 109$ ) of the observed pollen tubes, which showed a uniform distribution of the signal that also reached the pollen tube tip.

## Discussion

We report here that LARP6C, an evolutionarily conserved RBP, is essential for male fertility, acting during gametogenesis and germination and especially during the progamic phase, during which it is necessary for the directional growth of pollen tubes.

### The role of LARP6C in vesicular trafficking during male fertilization

The anisotropic growth of the pollen tube, which takes place exclusively at the apical dome, requires vast amounts of secretory vesicles delivered at the tip via cytoplasmic streaming. Golgi-derived secretory vesicles supply cell wall material as well as material for plasma membrane extension at the site of growth. Vesicles also deliver transmembrane proteins, such as receptor kinases, which are inserted into the apical plasma membrane through exocytosis (Grebnev et al., 2017). Indeed, the exocyst secretory complex was found to be essential for the specification of plasma

membrane nanodomains that define sites for the directional growth of pollen tubes (Synek et al., 2006, 2017; Li et al., 2010; Vukašinić and Žárský, 2016). We found that *larp6c*-pollen tubes are hypersensitive to BFA and identified several transcripts encoding components of the vesicular system as LARP6C mRNA clients, including factors involved in the trafficking of ER vesicles, constituents of the vacuolar trafficking system HOPS (Takemoto et al., 2018), components and regulators of the endosomal sorting complex required for transport (Reyes et al., 2014), and a subunit of the exocyst complex (Supplemental Data Set S1). We hence propose that the pollen tube guidance defects of *larp6c* mutants are in part the consequence of abnormal vesicular trafficking.

### LARP6C is necessary for lipid homeostasis during male fertilization

To optimize polar tip growth, pollen has evolved a unique lipid composition. In particular, pollen grains produce extraplastidial glycerolipids and store fatty acids and TAGs in LDs (Ischebeck, 2016). LDs are necessary for gametogenesis, pollen grain maturation, viability, and germination. They also might be required for pollen tube guided growth, as supported by the finding that MPK6 is a regulator of their synthesis involved in pollen tube guidance (Zhang et al., 2009, 2018). The exact role of LDs in pollen tubes is not currently clear, but it has been proposed that TAGs could be synthesized in the shank of the pollen tube and transported to the tip in the form of LDs to deliver membrane components (Ischebeck, 2016). In line with this idea, we report that LDs are distributed from shank to tip in the WT pollen tubes (Figure 4). Hence, the role of LARP6C in pollen tube guidance could also involve maintaining adequate LD levels, distribution, and possibly composition, as it can specifically bind mRNAs encoding fatty acid, TAG, phospho-, and glycerolipid synthases (FAD2, ACX4, TAG1, LPEAT2, MGD2) for lipases, such as SDP1, which is involved in storage lipid breakdown (Kelly et al., 2013), and for regulators of their synthesis, such as DYRK2A (Schulz-Raffelt et al., 2016) and MPK6 kinases (Zheng et al., 2018).

MGD2 is one of the three Arabidopsis synthases that catalyze the last step of MGDG synthesis. Consistent with the finding that galactolipids are unique and major constituents of plastid membranes, MGD1 and MGD3 were previously found to localize inside chloroplasts and at the periphery of plastids, respectively, which are consistent with a protein embedded in the outer envelope membrane. The subcellular

distribution in pollen tubes. The numbers of pollen tubes with gradient MGD2 distribution toward the tip, uniform (lost gradient), or no expression of MGD2-YFP are reported in the table below. Scale bars correspond to 10  $\mu\text{m}$ . C, Left panel: fluorescence quantification of MGD2-YFP in the WT and *larp6c-3* (*6c-3*) pollen and during the progamic phase (1 and 4 h).  $n = 3$  biological replicates at each time point, a Student's *t* test for two independent samples/two-tailed test was conducted, with ns, not significant; \*\*\*\* $P \leq 0.0001$ . Right panel: immunoblot analysis of endogenous levels of MGD2 in pollen and during progamic phase in the WT and *larp6c-3*. Experiments were conducted in two or three independent replicates labeled R1, R2, and R3. D, RT-qPCR analysis of MGD2 mRNA levels originating from the MGD2-YFP transgene and endogenous MGD2 gene in dry pollen and 4 h pollen tubes. Experiments were conducted in three independent replicates, and TUBULIN8 mRNA was used as a control. An unpaired Student's *t* test was conducted, with ns, not significant. Both the WT and *larp6c-3* express MGD2-YFP from the same primary transformant (line 6). In (A) and (B), the MGD2-YFP transgene is in the heterozygous state and the *larp6c-3* allele is homozygous. In (C) and (D), the WT and *larp6c-3* carry the MGD2-YFP transgene in the homozygous state

distribution of MGD2 was more difficult to interpret than that of its two counterparts, as it was detected in the cytosol (Awai et al., 2001). Here, in the absence of any plastid, we also report that MGD2 is present in the cytosol of the pollen tube and that it is distributed from shank to tip along a decreasing gradient that is lost in the absence of LARP6C. These observations uncover an unsuspected role for cytosolic MGD2, which could have the ability to produce MGDG outside plastids and possibly transport its substrate DAG to the site of MGDG synthesis. As MGDG is the substrate for DGDG, which was detected at the periphery of pollen tubes (Botté et al., 2011), MGD2 could participate to pollen tube membrane expansion. Alternatively, as DAG is also a substrate for TAG production, MGD2 may also transport this substrate to the sites of LD production and therefore participate to the guidance process. The changes in MGD2 protein levels and distribution along pollen tubes could hence be another reason for the observed guidance defect of the *larp6c* mutants.

On top of vesicular trafficking and lipid dynamics, LARP6C likely controls other cellular processes required for the directed growth of pollen tubes. Indeed, several LARP6C targets encode actors in processes involved in pollen tube elongation and guidance, such as signaling factors and kinases, cell wall modification players, or ion transporters. Moreover, some LARP6C clients were experimentally found to be involved in anisotropic cell elongation. These include, the transcription factor TFIIB1, which controls guided pollen tube growth (Zhou et al., 2013); TUB4, a structural microtubule component required for normal hypocotyl guidance and elongation (Yu et al., 2015); or the  $\alpha/\beta$  hydrolase-domain protein WAV2, which is involved in directional root growth (Mochizuki et al., 2005; Supplemental Data Set S1).

### Molecular functions of LARP6C during male fertilization

LARP6C is an RBP that physically interacts with PABP, a master regulator of mRNA translation and decay (Merret et al., 2013b). Here we demonstrated that LARP6C at least in part colocalizes with PABP in mature pollen grain. Furthermore, a LARP6C protein deficient in its RNA-binding domain (La-module) was unable to restore LARP6C's function in pollen tube guidance. We hence propose that LARP6C acts at the molecular level to control gene expression by regulating mRNA fate in the cytoplasm.

We provided strong evidence that LARP6C directly interacts with mRNAs harboring B-boxes of the B1 or B2 type in their 5'-UTRs (i.e. at least 52 of the 115 transcripts identified by RIP-seq; Supplemental Data Set S1). For some transcripts, only A-boxes were identified in the 5'-UTR. This might have occurred because we were only able to retrieve a partial 5'-UTR sequence, and inadvertently missed sequence regions that could contain the B-box, but it is also possible that some LARP6C RIP targets are in complex with this RBP but not through direct binding.

In *N. benthamiana* leaf epidermis, LARP6C appeared to control the levels of its mRNA targets as well as the amount of the corresponding translated proteins. LARP6C promoted the overaccumulation of YFP mRNA that carried its recognition sequence, specifically a B1-type B-box motif (Figure 6). We propose that at least in somatic cells, this overaccumulation is the result of LARP6C-mediated protection from cytoplasmic decay, rather than an action at the transcriptional level. Surprisingly, our results also show that this increase in mRNA levels is associated with a decrease in the corresponding YFP protein levels (Figure 8). This suggests that LARP6C could, while protecting its mRNA targets, dampen their translation. Alternatively, LARP6C could control protein stability, but since it is unlikely to interact with the reporter YFP protein (the only protein encoded by the reporter gene we designed), we deem this hypothesis unlikely. In eukaryotic cells, one common feature of mRNP granules is that they contain translationally silent mRNAs that are capable of (re)-entering translation in response to the appropriate signals and protect these mRNAs from decay (Buchan, 2014). Hence, the presence of LARP6C in foci that we propose are mRNP storage granules also rather favors the first hypothesis.

The mRNA stabilization effect of LARP6C binding observed in transient *N. benthamiana* assays is in contrast with the observation that in pollen grains, LARP6C does not seem to control its targets' steady-state levels. In pollen, as in animal gametes, mRNAs are highly stable, suggesting that in the male gametophyte, the mRNA decay machineries, as well as the translational apparatus, have poor activity (Ylstra and McCormick, 1999; Hafidh et al., 2018). This assumption is consistent with our observation that DCP1, a core constituent of the mRNA decapping complex, localizes to foci in mature pollen grains and that this localization is thought to be linked to quenched DCP1 activities. Indeed, work conducted in animal cells proposed that when components of the mRNA decay machineries are present in p-bodies, they are catalytically inactive (Hubstenberger et al., 2017). The discrepancies between the results from transient assays in *N. benthamiana* leaf cells and RNA-seq of pollen grains could hence be the consequence of differences in how the mRNA decay complex operates between sporophytic and reproductive cells.

In vivo, we propose that LARP6C plays a dual role in controlling of the levels of translated proteins encoded by its targets' transcripts. Using MGD2 mRNA as a model, we indeed showed that whilst antagonizing MGD2 protein accumulation in mature pollen grains, LARP6C promotes its translation after germination without affecting MGD2 mRNA levels (Figure 9). Although the possibility that LARP6C regulates the amount of MGD2 protein posttranslationally cannot be ruled out at this stage, we believe that it is unlikely, as discussed for the YFP reporter protein. This implies that LARP6C shifts from a repressor to an activator role in translation. This could be the result of a differential pattern of posttranslation modifications that might allow LARP6C to recruit different sets of accessory proteins to its

target mRNAs before and after pollen hydration, resulting in a mode switch from repression to activation.

Scarpin et al. (2017) reported that like *MGD2* mRNA, *SK14* mRNA is translationally silent in mature pollen grain and reactivated at germination. They also found that *SK14* mRNA aggregates in subcytoplasmic bodies that also contain the p-body component DCP1 (Scarpin et al., 2017). Here, we also demonstrated the existence of foci in mature pollen grain containing proteins that function in mRNA regulation (LARP6C and PAB5), which we believe also contain mRNAs. mRNP granules exist in most eukaryotes and in many cell types and are of different types based on their protein content. However, a common feature is that they store and protect translationally silent mRNPs until their protein product is needed. We therefore propose that a large portion of mRNAs whose expression is necessary for male fertilization are stored in mature pollen grains in the form of mRNP aggregates until their protein products are required during the progamic phase, as supported by previous findings (Hafidh et al., 2018), and that LARP6C is one of the trans-acting factors that orchestrate this process (see Supplemental Figure S9 for a summary model).

An intriguing observation from the current study is that LARP6C appears to be required for the distribution of the protein encoded by one of its client mRNAs, *MGD2*, along the pollen tube. We presently have no conclusive proof that LARP6C does not act at the protein level to participate in this gradient distribution. Nonetheless, considering that LARP6C is an mRNA-binding protein, we hypothesize that the defective distribution of *MGD2* in *larp6c* is the consequence of the aberrant regulation of its mRNA. We propose that LARP6C transports the translationally silent mRNAs present in mRNP granules to the appropriate cytoplasmic location where the protein is then translated and required. The existence of such localized translation events following the transport of silent mRNAs is a conserved and widespread feature of eukaryotes, including plants, where few examples of mRNAs targeted to the surface of the ER, chloroplasts, or mitochondria have been reported (Tian et al., 2020). In the vast majority of cases, mRNAs are transported by cytoskeletal motors in the form of silent mRNPs (Bullock, 2011; Elisovich and Singer, 2017). Consistent with a possible role in mRNA delivery, our data support the notion that LARP6C, in association with mRNP granules, likely navigates along microtubules in growing pollen tubes. Considering the phenotypes of *larp6c*-pollen, we propose that mRNA movement and localized translation are necessary for the polarized growth of pollen tubes and hence plant reproduction.

### The role of LARP6 proteins in mRNA control might be evolutionarily conserved

Interestingly, a recent study by Dermitt et al. demonstrated that human LARP6 acts in migrating cells to navigate mRNAs encoding RPs along microtubules to transport them from the cell body to protrusions; these cellular migrating fronts act as translation hotspots. This function of human

LARP6 in the spatiotemporal control of RP mRNA translation is necessary for cell proliferation and migration (Dermitt et al., 2020). The physiological roles of zebrafish LARP6 differ from that of Arabidopsis LARP6C, as it participates in oocyte development, chorion formation, and egg activation whilst it is not involved in male fertilization. Nevertheless, the authors suggest that zebrafish LARP6 could function in chorion formation by regulating mRNA metabolism in microvilli, that is, fine cell protrusions extending from both the developing oocytes and granulosa cells (Hau et al., 2020). It is interesting that LARP6 proteins, which are highly conserved eukaryotic RBPs, seem to have acquired distinct physiological roles during eukaryote evolution but could have retained their molecular mode of action in mRNA transport and translational control.

## Materials and methods

### Plant material and growth conditions

*Arabidopsis thaliana* ecotype Columbia-0 (Col-0) was used as the WT reference. The *larp6c-3* (SAIL\_268E02; McElver et al., 2001) and *larp6c-4* (WiscDsLox293-296invG4; Woody et al., 2007) lines were respectively ordered from the NASC and ABRC stock centers. Genotyping primers are shown in Supplemental Table S2. Stable transgenic lines were obtained using the *Agrobacterium tumefaciens*-based floral dip technique (Clough and Bent, 1998). For in vitro culture, surface sterilized seeds were sown on synthetic Murashige & Skoog (MS) medium at 2.20 g·L<sup>-1</sup> (1/2 MS) with 0.8% agar and stored for 48 h at 4°C in the dark before being grown under continuous light (50–60 μE·m<sup>-2</sup>·s<sup>-1</sup>) at 20°C. Plants in soil cultures were grown in growth chambers under a 16 h light (100 μE·m<sup>-2</sup>·s<sup>-1</sup>)/8 h dark cycle at 20°C with approximately 75% humidity. See “Supplemental methods” for growth conditions used to collect mature pollen for RNA-seq and RIP-seq experiments.

### Cloning and plasmids

All LARP6C-containing fusion proteins (YFP, TagRFP, and FLAGHA) were expressed under the control of the upstream genomic sequences (spanning region –1181 to –1 from ATG) of the *LARP6C* gene (*AT3G19090* locus). To obtain the LARP6C-tRFP and LARP6C-FLAGHA fusions, we isolated total genomic DNA from Col-0 and PCR amplified the *LARP6C* genomic region starting from nucleotide –1181 from the ATG to the last nucleotide before the stop codon using primers 543 and 544 (Supplemental Table S2). The PCR product was inserted at sites *KpnI* and *NheI* upstream of either the tagRFP or FLAG-HA tag into a pCambia (1300-based plant binary vector expressing the *HPTII* (hygromycin) resistance gene, giving rise to vectors pEB16 and pEB13. To obtain the YFP-LARP6C expressing binary vector, the genomic region spanning nucleotides –1181 to –1 from the ATG of the *LARP6C* gene was PCR amplified with primers 974 and 975 from vector pEB13 and cloned at sites *SacI* and *KpnI* upstream of a Gateway entry cassette into a pZP221-based (Hajdukiewicz et al., 1994) plant

binary vector carrying the AAC1 (gentamycin) resistance gene, giving rise to vector p788. The *LARP6C* coding genomic region was PCR amplified from total genomic DNA with primers 976–977 and cloned at sites *SpeI-EcoRV* downstream of the YFP tag located between the *AttL1* and *L2* Gateway donor sites, giving rise to plasmid p793. The plant binary vector p795 was obtained through a Gateway cloning reaction between p788 and 793. The *PAB5* genomic sequence (–1966 from the ATG to the last nucleotide before the stop codon) was PCR amplified from total genomic DNA with primers eb3 and eb4 and cloned using the restriction endonucleases *XbaI* and *BamHI* into vector CTL579 (pCAMBIA-1300) upstream of the GFP tag, giving rise to plasmid pEB3. To prepare transgenic lines expressing the YFP-*LARP6CΔLAM* protein, we transformed *larp6c-3* or *larp6c-4* plants with plasmid p844. The *LARP6CΔLAM* CDS codes for a *LARP6C* protein deleted of the region spanning amino acids 137–227 were obtained as follows. We PCR amplified the regions of the coding sequence from +1 to +411 from ATG (primers 1197 and 1198) with primer 1198, which also adds a 3′-tail extension of 20 nt complementary to region 684–704 of the CDS (located just downstream to the LAM). A second PCR product was generated with primers 1199–1200, starting from position 684 to the stop codon. To fuse both products, we ran a third PCR amplification with primers 1201–1200 and an equimolar mixture of products 1 and 2 as a matrix. The resulting fragment corresponds to the full-length *LARP6C* CDS deleted of its LAM and carrying *XbaI* and *EcoRV* restriction sites at its 5′ and 3′ ends, respectively. This fragment was inserted downstream of the YFP sequence into a Gateway donor vector through enzymatic restriction and ligation (p843). The YFP-*LARP6CΔLAM* fusion construct was transferred into a plant binary vector under the control of the *LARP6C* native promoter through Gateway cloning between p843 and p788 (p844).

The binary vector pGEX2-GEX2GFP was obtained from Mori et al. (2014). Binary plasmids for transient assays were prepared as follow. DNA fragments encompassing a basal CaMV35S promoter without enhancer sequences (Töpfer et al., 1987), modified *MGD2* 5′-UTRs, and the YFP CDS were ordered from GeneCust (<http://www.genecust.com/fr>) and subcloned into a Gateway donor vector. DNA cassettes were then introduced into a plant binary vector containing the *HPTII* (hygromycin) resistance gene (vector CTL575, a derivative of pCAMBIA-1300). The *LARP6C* coding sequence was fused downstream of the tagRFP fluorescent reporter and placed under the control of a strong CaMV35S promoter by Gateway recombination with the plant binary entry vector p-SITE-6C1 (Martin et al., 2009).

To prepare a translational *MGD2*-YFP fusion, we amplified the *MGD2* genomic region starting from nucleotide –579 from the ATG to the last nucleotide before the stop codon using primers 31 and 32 (Supplemental Table S2). The complete PCR product was cloned into pDONR221 via the TOPOisomerase cloning technique to generate entry vector

pDONR221-*MGD2*no-stop. To generate the plant expression vector, LR Clonase was used to recombine pDONR221-*MGD2*no-stop into the pB7FWG,0 Gateway binary vector in frame with C-terminal YFP. Primary transformants were selected using BASTA selection.

### Pollen phenotyping

Pollen transmission tests were conducted through hand pollination of the WT pistils with pollen from mutant and complemented homozygous plants. The number of offspring carrying the mutation was scored either by PCR-based genotyping or by selection of antibiotic/herbicide-resistant seedlings. The number of mutant seedlings was expressed as a percentage over the total number of seedlings and TE of the mutant gametophyte calculated as  $asTE = \left( \left( \frac{\text{No.ofmutant}}{\text{No.ofWT}} \right) \times 100 \right)$ . Experiments were conducted in triplicate. Pollen tube guidance efficiency was scored either by SIV (Palanivelu and Preuss, 2006) or in vivo assays by observing pistils hand pollinated with the mutant pollen of interest and stained with aniline blue (Mori et al., 2006). Emasculated pistils were from *ms1* (male sterility 1) heterozygous plants. This guaranteed that the pistils were not contaminated with the WT pollen, as the *ms1-1* mutant is male sterile (van der Veen and Wirtz, 1968; Ito et al., 2007). Monitoring of pollen tube guidance in the presence of galvestine-1 was conducted through SIV assays on plates containing 1% DMSO for mock treatment or 5 or 10 μM of galvestine-1 with a final concentration of 1% DMSO. For all pollen tube guidance assays, in vivo aniline blue staining and SIV as well as in vivo blue dot assays were performed according to Kulichová et al. (2020).

### Pollen and pollen tube collection for total RNA and protein extraction

Approximately 250 μL equivalent of open flowers were collected in 1.5-mL Eppendorf tubes for each respective genotype. To collect mature pollen, flowers were vigorously and briefly vortexed with 500 μL of RIPA extraction buffer for protein extraction or with pollen germination medium for RNA extraction and spun in a benchtop centrifuge for 1 min. Media were removed and pellets stored at –80°C until extraction. For pollen activation/germination, the pollen pellet was resuspended in liquid pollen germination medium and incubated for 1 h at 22°C. One biological replicate corresponds to one sample of 250 μL equivalent of open flowers.

### Microscopy

Subcellular localization experiments in pollen grain and pollen tubes were conducted with an LSM700 confocal microscope (Zeiss) using emission/excitation wavelengths: 405 nM/420–480 nM for DAPI, 555 nM/600–700 nM for tRFP, and 488 nM/490–555 nM for YFP and GFP. Mature pollen grains were collected by dipping open flowers into a drop of DAPI solution (1× PBS pH 7, 0.5% Triton-X100, 1 μg·mL<sup>-1</sup>

4',6-diamino-2-phenylindole) on a glass slide. To collect immature pollen grains at the microspore, bicellular and tricellular stages, anthers were collected from unopened buds, placed in a drop of DAPI solution on a glass slide, and gently crushed to free the pollen grains from pollen sacs. Pollen tubes germinated and grown as described in the [Supplemental Methods](#) were directly observed from the germination slide. For cytoskeleton colocalization, PRO<sub>LARP6C</sub>-tRFP:LARP6C was coinfiltrated in *N. benthamiana* leaves with either p35S:GFP-AtTUB6, p35S:GFP-FABD2, or pUBQ-LifeAct:GFP. Confocal images were taken under a Nikon Eclipse Ti confocal microscope equipped with a CSU-X1 spinning disk module and Andor iXon3 EMCCD camera, as well as with a Zeiss LSM880 confocal microscope, and captured with ZEN 2.3v software. Images were analyzed and assembled with ImageJ/Fiji (<http://imagej.net/http://fiji.sc/Fiji>), Adobe Photoshop CS6 ([www.adobe.com](http://www.adobe.com)), Inkscape ([www.inkscape.org](http://www.inkscape.org)), and NIS Elements (LIM) software. For YFP quantification in pollen tubes, MGD2-YFP signals in the respective genotypes were captured under a Zeiss LSM880 confocal microscope using an Argon 488 laser and detected with GasP detector with fixed configurations. Zen (blue edition) software was used to quantify pixel intensity, and data were processed in Excel.

### Pharmacological treatment

For the galvestine-1 inhibition assay, pollen tubes were grown on solid pollen germination medium containing 1% DMSO for mock treatment or 5 or 10  $\mu\text{M}$  of galvestine-1 at a final concentration of 1% DMSO. For BFA A treatment, Arabidopsis pollen tubes were grown for 1 h in vitro and stained by incubating with 1- $\mu\text{M}$  FM4-64 (Thermo Fisher Scientific, <https://www.thermofisher.com>) concomitantly with BFA at 25  $\mu\text{M}$  (Sigma, [www.sigmaaldrich.com](http://www.sigmaaldrich.com), BFA stock solution at 50 mM in DMSO) in liquid pollen germination medium for 5 and 10 min. To visualize LDs, Bodipy stain (505/515) at a final concentration of 2  $\mu\text{M}$  and Nile red stain (552/636) at a final concentration of (0.1  $\mu\text{g}\cdot\text{mL}^{-1}$ ) were simultaneously added to germinated pollen tubes and incubated for 3 min prior to imaging.

### Total RNA extraction and RT-qPCR

For RNA-sequencing purpose, total RNA was purified from mature pollen grain as follow. Around 0.5–3 mg of dry pollen was ground with a Silamat S6 mixing device (Ivolcar Vivadent, Schaan, Liechtenstein) in 500  $\mu\text{L}$  of GuHCl buffer (8-M GuHCl, 20-mM MES, 20-mM EDTA, at pH 7, 50-mM  $\beta$ -mercaptoethanol) and with five glass beads. Following 1 min vortexing at full speed and 10 min incubation on ice, RNAs were separated from proteins via two consecutive phenol–chloroform–isoamyl alcohol (IAA, 25:24:1) extractions, followed by one extraction with chloroform–IAA (24:1), consisting of 1 min vortexing at full speed and 10-min centrifugation at 16°C, 14,000g. RNAs are then precipitated in the presence of 0.7 vol. isopropanol, 1/20th  $\text{CH}_3\text{COOH}$  at 1 M for 20 min at  $-20^\circ\text{C}$ . Following 20-min centrifugation at 4°C, 14,000g, the RNA pellet was washed

in 90% EtOH and resuspended in RNase free water. The average efficiency of pollen RNA extraction was 5–6  $\mu\text{g}$  of RNA per mg of dry pollen. To measure MGD2 (YFP-MGD2 and endogenous MGD2) mRNA levels, total RNA was extracted from 5 mg of dry pollen and 250  $\mu\text{L}$  equivalent of flowers used to grow pollen tubes for 4 h in vitro from (MGD2-YFP; LARP6C) and (MGD2-YFP; *lar6c-3*) homozygous lines. One biological replicate corresponds to 5 mg of dry pollen and 250  $\mu\text{L}$  equivalent flowers for pollen tubes. A total of three biological and six technical replicates were generated. MGD2 native primers and TUB8 were used for measurement and normalization, respectively. Relative expression was computed as above.

To quantify YFP mRNA levels in *N. benthamiana* transient assays, total RNA was isolated from the samples using a Monarch Total RNA Miniprep Kit (New England Biolabs), and genomic DNA was eliminated using gDNA removal columns and on-column DNaseI-treated (New England Biolabs). Five micrograms of total RNA were reverse transcribed with a SuperScript IV kit (Life Technology) using an oligodT<sub>18</sub> primer. qPCR was conducted on a LightCycler 480 Multiwell Plates 384-well thermocycler (Roche Applied Sciences) with the following amplification program: 5 min 95°C, 40 cycles of 15 s at 95°C, and 1 min at 60°C. After amplification, melting curve analysis was performed with a temperature gradient of 0.1°C·s<sup>-1</sup> from 60°C to 95°C. The PCR mixture contained Takyon qPCR master mix (Eurogentec), 500-nM gene-specific primers, and 1- $\mu\text{L}$  cDNA in a total reaction volume of 10  $\mu\text{L}$ . Primer efficiencies were determined using standard curves, with 10-fold serial dilution series ranging from  $1 \times 10^1$  to  $1 \times 10^6$  of the cDNA samples. Relative quantification was performed by the  $\Delta\Delta\text{C}_T$  method (Livak and Schmittgen, 2001), with YFP and HPTII used as the target and reference gene, respectively. The sequences of the primers used for RT- and qPCR are shown in [Supplemental Table S2](#).

### RNA-seq, RIP-seq, bioinformatics

Techniques related to large-scale analyses (RNA-seq and RIP-seq), as well as the bioinformatic analyses, are detailed in the [“Supplemental methods.”](#)

### Protein-related techniques

Total protein extracts were separated by sodium dodecyl sulphate–polyacrylamide gel electrophoresis (SDS–PAGE) on an acrylamide gel before being electrotransferred onto a PVDF membrane (0.45  $\mu\text{M}$ , Merck Millipore). After saturation in a (1× TBS – 0.1% tween – 5% fat-free dry milk) solution, the membranes were incubated with the appropriate primary then secondary antibodies, washed three times with a 1× TBS – 0.1% Tween solution, and chemiluminescence revealed with an EMD Millipore Immobilon Western Chemiluminescent HRP Substrate kit. Antibodies against the LARP6C protein were custom made (at Agro-Bio, La Ferté St Aubin, France) through immunization of rabbits with the peptide “KRTSQFTDRDREELGQ” (amino acids 220–235). Anti-LARP6C antibodies are utilized at 1/1,000 dilution in a

(1× TBS – 0.1% Tween – 5% fat-free dry milk) solution and incubated overnight at 4°C with gentle shaking. Secondary antibodies were anti-rabbit HRP (Bio-Rad) and used at a 1/5,000 dilution. Anti-ACTIN antibodies were from Affinity Bio Reagents (Golden, CO, USA) and used at 1/15,000 dilution. Secondary antibodies were anti-mouse HRP (Bio-Rad) used at a 1/10,000 dilution. For transient assays, the YFP protein was detected using the GFP antibody (Clontech) at 1/5,000 and the UGPase antibody (Agrisera) at 1/7,500 dilution, both incubated overnight at 4°C. Secondary antibodies anti-mouse HRP (Bio-Rad) used at a 1/2,000 dilution and anti-rabbit HRP (Bio-Rad) used at a 1/5,000 dilution were incubated for YFP and UGPase detection, respectively, for 1h at room temperature. To detect endogenous MGD2, proteins were extracted from 5 mg of dry pollen and 250 µL equivalent of flowers used to germinate pollen tubes in vitro for 1h or 4h from (MGD2-YFP; LARP6C) and (MGD2-YFP; *larp6c-3*) homozygous lines. One biological replicate corresponds to 5 mg of pollen grain, and 250 µL equivalent open flowers for pollen tubes. A total of three replicates for dry pollen and 1 h activated pollen, and two replicates for 4 h pollen tubes were generated. After SDS–PAGE separation, membrane blocking was performed with 5% milk for 30 min at room temperature. The membrane was incubated with antibodies against MGD2 (a gift from Eric Maréchal [LPCV, Grenoble]; [Awai et al., 2001](#)), at 1/500 dilution, overnight at 4°C. Secondary anti-Rabbit HRP (Agrisera) was used at 1/10,000 dilution and incubated for 1 h at room temperature prior to membrane development.

For RNA-protein binding in vitro assays, the LARP6C La-module (amino acids 137–223) was recombinantly expressed as in [Merret et al. \(2013b\)](#). The hexahistidine tag (His-tag) was removed by proteolysis via incubation at 4°C overnight with HRV 3C Protease in a buffer containing 50-mM Tris-HCl, pH 7.25, 100-mM KCl, 0.2-mM EDTA, 1-mM DTT, 10% glycerol. The cleaved His-Tag and the protease were separated from the La-module through retention onto a Ni-NTA column. The protein was then subjected to heparin column purification and dialysis in a final buffer as in [Merret et al. \(2013b\)](#).

### ITC and EMSA

RNA oligos were custom made from IBA-Lifescience GmbH (Göttingen, Germany) at a 1-µM molar scale and HPLC purified. The lyophilized RNAs were resuspended in RNase free water (DEPC treated) at concentrations ranging from 2.5 to 3 mM. The ITC experiments were performed as in [Merret et al. \(2013b\)](#) on an iTC200 microcalorimeter (Malvern). Here, 20 injections of 2-µL RNA solutions at 200–320 µM concentration were added to protein solutions (LARP6C La-module) at 20–30 µM with a computer-controlled 40-µL syringe. Control titrations of RNA into buffer alone and into protein solution without the His-tag were performed. The heat per injection normalized per mole of injectant versus molecular ratio was analyzed with the MicroCal-Origin 7.0 software package and fitted using a nonlinear least-square minimization algorithm using a theoretical single-site binding model.

$\Delta H$  (reaction enthalpy change in kcal·mol<sup>-1</sup>),  $K_b$  (binding constant equal to 1/Kd), and  $n$  (molar ratio between the two proteins in the complex) were the fitting parameters. The reaction entropy was calculated using the equations  $\Delta G = -RT \ln K_b$  ( $R = 1.986 \text{ cal}\cdot\text{mol}^{-1} \text{ K}^{-1}$ ;  $T = 298 \text{ K}$ ) and  $\Delta G = \Delta H - T\Delta S$ . All ITC experiments were repeated at least three times, and a detailed analysis of the thermodynamic parameters and errors calculated as the standard deviation from the mean value are reported in [Supplemental Table S1](#). For EMSA, RNAs were 5'-labeled with  $\gamma$ -<sup>32</sup>P-ATP using T4 polynucleotide kinase. Recombinant protein and RNA were mixed and incubated for 15 min at room temperature in 20-mM Tris, pH 7.25, 200-mM KCl, 5% of glycerol, 1-mM DTT, 0.1 mg·mL<sup>-1</sup> of BSA and 0.7 units of RNase inhibitors (RNaseOUT, Invitrogen). Each reaction mixture (22 µL) contained 3 nM of labeled RNA oligo and varying amounts of LARP6C La-module (3-fold serial dilutions from an 88-µM sample). The experiments were performed in the absence or presence of unlabeled mixed tRNAs from *E. coli* MRE 600 (0.01 mg·mL<sup>-1</sup>). After the addition of 2 µL of 30% Ficoll, the samples were loaded on a 9% native polyacrylamide gel prerun at 100 mV for 1 h at 4°C in 0.5× Tris-borate-EDTA buffer. A typical EMSA experiment was run at 4°C for 1 h at 125 mV. Gels were dried onto 3MM chromatography paper, exposed to a phosphoimaging plate overnight, analyzed on a Typhoon Trio phosphoimager, and quantified with Image Quant TL software. The fraction of bound RNA was plotted versus the protein concentrations. To determine the dissociation constants, the data were fitted with Origin 8.0 to a modified Hill equation ([Ryder et al., 2008](#)) using nonlinear least squares methods and assuming a 1:1 stoichiometry.

### *Nicotiana benthamiana* transient assays

Plasmids B1-YFP, B3-YFP, and RFP-LARP6C were respectively transformed into *A. tumefaciens* strain LB4404. Transformed bacteria were cultivated until they reached OD 0.8 and used to infiltrate fully expanded leaves from 8-week-old *N. benthamiana* plants using a needleless syringe as described in [Ruiz et al. \(1998\)](#). When double transformations were performed (B1-YFP and RFP-LARP6C or B3-YFP and RFP-LARP6C), an equimolar mixture of *Agrobacterium* cultures (OD 0.4) was used for transformation. For each transformation, we also used an *Agrobacterium* culture carrying a plasmid (OD 0.2) allowing the expression of the P19 suppressor of RNA silencing ([Lasierra and Prat, 2018](#)). Three days postinfiltration (dpi), transformed leaf segments were collected, flash frozen, and total RNA or protein extracted. Alternatively, at 3 dpi transformed leaves were observed by confocal microscopy to monitor YFP and tRFP signals.

### Accession numbers

Sequence data in this study can be found under the following accession numbers: Bioproject PRJNA557669. RNA-Seq-Col0-Rep 1: SRR9887494; RNA-Seq-Col0-Rep 1: SRR9887493; RNA-Seq-*larp6c-3*-Rep 1; SRR9887496; RNA-Seq-*larp6c-3*-Rep 2

SRR9887495; RIP-Col0-Input-Rep 1: SRR9887498; RIP-Col0-Euate-Rep 1: SRR9887500; RIP-Col0-Input-Rep 2: SRR9887497; RIP-Col0-Euate-Rep 2: SRR9887499; RIP-LARP6C-Input-Rep 1: SRR9887490; RIP-LARP6C-Euate-Rep 1: SRR9887492; RIP-LARP6C-Input-Rep 2: SRR9887489; RIP-LARP6C-Euate-Rep 2: SRR9887491.

## Supplemental data

The following materials are available in the online version of this article.

**Supplemental Figure S1.** Expression profiles of *LARP6A*, *6B*, and *6C* mRNAs across development.

**Supplemental Figure S2.** Pollen maturation, germination, and pollen tube growth of *larp6c* lof mutants.

**Supplemental Figure S3.** Schematic representation of *LARP6C* transgenes, immunoblotting analyses of their accumulation, SIV pollen tube guidance competition assays, and analysis of *LARP6A* function in male fertilization.

**Supplemental Figure S4.** Pollen attraction competence of *larp6c-3* and *6c4* ovules.

**Supplemental Figure S5.** Confocal analyses of *LARP6C*-tRFP and *LARP6A*-GFP in pollen.

**Supplemental Figure S6.** Reproducibility of the RIP-seq data, RIP-seq filtering workflow, representation of the position of A and/or B boxes on the 5'-UTRs of *LARP6C* targets.

**Supplemental Figure S7.** ITC and EMSA assessment of *LARP6C* La-module binding to A-type oligos.

**Supplemental Figure S8.** Reproducibility of the RNA-seq data.

**Supplemental Figure S9.** Model of the molecular functions of *LARP6C* in male fertilization.

**Supplemental Table S1.** Thermodynamic parameters of the calorimetric analyses shown in Figure 4, B and D; Supplemental Figure 6A.

**Supplemental Table S2.** List and sequences of primers used for q-PCR, genotyping, and cloning.

Supplemental Methods

**Supplemental Data Set S1.** Results of RIP-seq experiment.

**Supplemental Data Set S2.** Results of RNA-Seq experiment.

**Supplemental Movie S1.** *LARP6C* foci move along microtubules.

## Acknowledgments

We thank David Twell group (Leicester University) for sharing LAT52:H2B-GFP marker, Martin Potoský (Cell Biology, IEB Prague), Eva Kollárová, and Fatima Cvrčková (Faculty of Science, Charles University, Prague) for the cytoskeleton constructs. The authors would like to thank Eric Maréchal (LPCV, Grenoble) for sharing MGD2 antibodies and galvestine-1, as well as for fruitful discussions on *LARP6C* targets' functions, in particular those involved in lipid biology.

## Funding

This work was funded by the CNRS, The University of Perpignan (UPVD), the Agence Nationale pour la Recherche (ANR) grant Heat-EpiRNA (grant no. ANR-17-CE20-007-01); a Bonus Quality Research (BQR) funded by the University of Perpignan; a Collaborative PICS Project (LARP&STRESS, grant no. 6170) funded by CNRS; Grantová agentura České republiky (GACR; grant nos. 17-23203S and 18-02448S), European Regional Development Fund-Project “Centre for Experimental Plant Biology” (No. CZ.02.1.01/0.0/0.0/16\_019/0000738) and the Royal Society Newton International fellowship (ref. NF140482). This study is set within the framework of the “Laboratoires d’Excellence (LABEX)” TULIP (ANR-10-LABX-41). E.B. was the recipient of a PhD grant from the UPVD, Doctoral School ED305. C.G.L. Jr is the recipient of a short-term contract supported by the ANR Heat-EpiRNA (ANR-17-CE20-007-01). S.H., K.K., and D.H. are supported by GACR (grant nos. 17-23203S and 18-02448S). S.H. is also supported by European Regional Development Fund-Project “Centre for Experimental Plant Biology” (grant no. CZ.02.1.01/0.0/0.0/16\_019/0000738). I.C.G. was supported by a Royal Society Newton International fellowship (ref. NF140482). I.G.C. and M.R.C. thank the Centre for Biomolecular Spectroscopy at King’s College London funded by a capital award from the Wellcome Trust.

*Conflict of interest statement.* None declared.

## References

- Ambrose JC, Cyr R (2007) The Kinesin ATK5 functions in early spindle assembly in Arabidopsis. *Plant Cell* **19**: 226–236
- Awai K, Maréchal E, Block MA, Brun D, Masuda T, Shimada H, Takamiya K, Ohta H, Joyard J (2001) Two types of MGDG synthase genes, found widely in both 16:3 and 18:3 plants, differentially mediate galactolipid syntheses in photosynthetic and non-photosynthetic tissues in Arabidopsis thaliana. *Proc Natl Acad Sci USA* **98**: 10960–10965
- Belostotsky DA (2003) Unexpected complexity of poly(A)-binding protein gene families in flowering plants: three conserved lineages that are at least 200 million years old and possible auto- and cross-regulation. *Genetics* **163**: 311–319
- Belostotsky DA, Meagher RB (1996) A pollen-, ovule-, and early embryo-specific poly(A) binding protein from Arabidopsis complements essential functions in yeast. *Plant Cell* **8**: 1261–1275
- Botella C, Sautron E, Boudiere L, Michaud M, Dubots E, Yamaryo-Botté Y, Albrieux C, Marechal E, Block MA, Jouhet J (2016) ALA10, a phospholipid flippase, controls FAD2/FAD3 desaturation of phosphatidylcholine in the ER and affects chloroplast lipid composition in Arabidopsis thaliana. *Plant Physiol* **170**: 1300–1314
- Botté CY, Deligny M, Rocchia A, Bonneau A-L, Saïdani N, Hardré H, Aci S, Yamaryo-Botté Y, Jouhet J, Dubots E, et al. (2011) Chemical inhibitors of monogalactosyldiacylglycerol synthases in Arabidopsis thaliana. *Nat Chem Biol* **7**: 834–842
- Bousquet-Antonelli C, Deragon J-M (2009) A comprehensive analysis of the La-motif protein superfamily. *RNA* **15**: 750–764
- Brownfield L, Hafidh S, Borg M, Sidorova A, Mori T, Twell D (2009) A plant germline-specific integrator of sperm specification and cell cycle progression. *PLoS Genet* **5**: e1000430
- Buchan JR (2014) mRNP granules. Assembly, function, and connections with disease. *RNA Biol* **11**: 1019–1030

- Bullock SL** (2011) Messengers, motors and mysteries: sorting of eukaryotic mRNAs by cytoskeletal transport. *Biochem Soc Trans* **39**: 1161–1165
- Cai L, Fritz D, Stefanovic L, Stefanovic B** (2010a) Binding of LARP6 to the conserved 5' stem-loop regulates translation of mRNAs encoding type I collagen. *J Mol Biol* **395**: 309–326
- Cai L, Fritz D, Stefanovic L, Stefanovic B** (2010b) Nonmuscle myosin-dependent synthesis of type I collagen. *J Mol Biol* **401**: 564–578
- Challa AA, Stefanovic B** (2011) A novel role of vimentin filaments: binding and stabilization of collagen mRNAs. *Mol Cell Biol* **31**: 3773–3789
- Clough SJ, Bent AF** (1998) Floral dip: a simplified method for *Agrobacterium*-mediated transformation of *Arabidopsis thaliana*. *Plant J* **16**: 735–743
- Cvrčková F, Oulehlová D** (2017) A new kymogram-based method reveals unexpected effects of marker protein expression and spatial anisotropy of cytoskeletal dynamics in plant cell cortex. *Plant Methods* **13**: 19
- Dermit M, Dodel M, Lee FCY, Azman MS, Schwenzer H, Jones JL, Blagden SP, Ule J, Mardakheh FK** (2020) Subcellular mRNA localization regulates ribosome biogenesis in migrating cells. *Dev Cell* **55**: 298–313.e10
- Eliscovich C, Singer RH** (2017) RNP transport in cell biology: the long and winding road. *Curr Opin Cell Biol* **45**: 38–46
- Feng Q-N, Liang X, Li S, Zhang Y** (2018) The ADAPTOR PROTEIN-3 complex mediates pollen tube growth by coordinating vacuolar targeting and organization. *Plant Physiol* **177**: 216–225
- Grebnev G, Ntefidou M, Kost B** (2017) Secretion and endocytosis in pollen tubes: models of tip growth in the spot light. *Front Plant Sci* **8**: 154
- Hafidh S, Potěšil D, Fíla J, Feciková J, Čapková V, Zdráhal Z, Honys D** (2014) In search of ligands and receptors of the pollen tube: the missing link in pollen tube perception. *Biochem Soc Trans* **42**: 388–394
- Hafidh S, Potěšil D, Müller K, Fíla J, Michailidis C, Herrmannová A, Feciková J, Ischebeck T, Valášek LS, Zdráhal Z, et al.** (2018) Dynamics of the pollen sequestrome defined by subcellular coupled omics. *Plant Physiol* **178**: 258–282
- Hajdukiewicz P., Svab Z., and Maliga P.** (1994) The small, versatile pZP family of *Agrobacterium* binary vectors for plant transformation. *Plant Mol. Biol.* **25**: 989–994
- Hau HTA, Ogundele O, Hibbert AH, Monfries CAL, Exelby K, Wood NJ, Nevarez-Mejia J, Carbajal MA, Fleck RA, Dermit M, et al.** (2020) Maternal Larp6 controls oocyte development, chorion formation and elevation. *Development* **147**: dev187385
- Hellman LM, Fried MG** (2007) Electrophoretic mobility shift assay (EMSA) for detecting protein–nucleic acid interactions. *Nat Protoc* **2**: 1849–1861
- Higashiyama T, Takeuchi H** (2015) The mechanism and key molecules involved in pollen tube guidance. *Annu Rev Plant Biol* **66**: 393–413
- Honys D, Combe JP, Twell D, Capková V** (2000) The translationally repressed pollen-specific ntp303 mRNA is stored in non-polysomal mRNPs during pollen maturation. *Sex Plant Reprod* **13**: 135–144
- Honys D, Twell D** (2004) Transcriptome analysis of haploid male gametophyte development in *Arabidopsis*. *Genome Biol* **5**: R85
- Hubstenberger A, Courel M, Bénard M, Souquere S, Ernoult-Lange M, Chouaib R, Yi Z, Morlot JB, Munier A, Benard M, et al.** (2017) P-body purification reveals the condensation of repressed mRNA regulons. *Mol Cell* **68**: 144–157.e5
- Ischebeck T** (2016) Lipids in pollen—they are different. *Biochim Biophys Acta* **1861**: 1315–1328
- Ito T, Nagata N, Yoshida Y, Ohme-Takagi M, Ma H, Shinozaki K** (2007) *Arabidopsis* MALE STERILITY1 encodes a PHD-type transcription factor and regulates pollen and tapetum development. *Plant Cell* **19**: 3549–3562
- Johnson MA, Preuss D** (2002) Plotting a course: multiple signals guide pollen tubes to their targets. *Dev Cell* **2**: 273–281
- Kelly AA, van Erp H, Quettier A-L, Shaw E, Menard G, Kurup S, Eastmond PJ** (2013) The SUGAR-DEPENDENT1 lipase limits triacylglycerol accumulation in vegetative tissues of *Arabidopsis*. *Plant Physiol* **162**: 1282–1289
- Khan BR, Adham AR, Zolman BK** (2012) Peroxisomal acyl-CoA oxidase 4 activity differs between *Arabidopsis* accessions. *Plant Mol Biol* **78**: 45–58
- Klepikova AV, Logacheva MD, Dmitriev SE, Penin AA** (2015) RNA-seq analysis of an apical meristem time series reveals a critical point in *Arabidopsis thaliana* flower initiation. *BMC Genomics* **16**: 466
- Kulichová K, Kumar V, Steinbachová L, Klodová B, Timofejeva L, Juříček M, Honys D, Hafidh SS** (2020) PRP8A and PRP8B spliceosome subunits act coordinately to control pollen tube attraction in *Arabidopsis thaliana*. *Development* **147**: dev186742
- Lasierra P, Prat S** (2018) Transient reactivation studies in *Nicotiana benthamiana* leaves. *Methods Mol Biol* **1794**: 311–322
- Li S, van Os GMA, Ren S, Yu D, Ketelaar T, Emons AMC, Liu C-M** (2010) Expression and functional analyses of EXO70 genes in *Arabidopsis* implicate their roles in regulating cell type-specific exocytosis. *Plant Physiol* **154**: 1819–1830
- Livak KJ, Schmittgen TD** (2001) Analysis of relative gene expression data using real-time quantitative PCR and the 2<sup>-ΔΔCT</sup> method. *Methods* **25**: 402–408
- Manojlovic Z, Earwood R, Kato A, Perez D, Cabrera OA, Didier R, Megraw TL, Stefanovic B, Kato Y** (2017) LA-related protein 6 controls ciliated cell differentiation. *Cilia* **6**: 4
- Maraia RJ, Mattijssen S, Cruz-Gallardo I, Conte MR** (2017) The La and related RNA-binding proteins (LARPs): structures, functions, and evolving perspectives. *Wiley Interdiscip Rev RNA* **8**: e1430
- Martin K, Kopperud K, Chakrabarty R, Banerjee R, Brooks R, Goodin MM** (2009) Transient expression in *Nicotiana benthamiana* fluorescent marker lines provides enhanced definition of protein localization, movement and interactions in planta. *Plant J* **59**: 150–162
- Martino L, Pennell S, Kelly G, Busi B, Brown P, Atkinson RA, Salisbury NJ, Ooi ZH, See KW, Smerdon SJ, et al.** (2015). Synergic interplay of the La motif, RRM1 and the interdomain linker of LARP6 in the recognition of collagen mRNA expands the RNA binding repertoire of the La module. *Nucleic Acids Res* **43**: 645–660
- McCue AD, Cresti M, Feijó JA, Slotkin RK** (2011) Cytoplasmic connection of sperm cells to the pollen vegetative cell nucleus: potential roles of the male germ unit revisited. *J Exp Bot* **62**: 1621–1631
- McElver J, Tzafirir I, Aux G, Rogers R, Ashby C, Smith K, Thomas C, Schetter A, Zhou Q, Cushman MA, et al.** (2001). Insertional mutagenesis of genes required for seed development in *Arabidopsis thaliana*. *Genetics* **159**: 1751–63.
- Merret R, Descombin J, Juan Y-T, Favory J-J, Carpentier M-C, Chaparro C, Charng Y-Y, Deragon J-M, Bousquet-Antonelli C** (2013a). XRN4 and LARP1 are required for a heat-triggered mRNA decay pathway involved in plant acclimation and survival during thermal stress. *Cell Rep* **5**:1279–1293
- Merret R, Martino L, Bousquet-Antonelli C, Fneich S, Descombin J, Billey É, Conte MR, Deragon J-M** (2013b) The association of a La module with the PABP-interacting motif PAM2 is a recurrent evolutionary process that led to the neofunctionalization of la-related proteins. *RNA* **19**: 36–50
- Mochizuki S, Harada A, Inada S, Sugimoto-Shirasu K, Stacey N, Wada T, Ishiguro S, Okada K, Sakai T** (2005) The *Arabidopsis* WAVY GROWTH 2 protein modulates root bending in response to environmental stimuli. *Plant Cell* **17**: 537–547
- Mori T, Igawa T, Tamiya G, Miyagishima S-Y, Berger F** (2014) Gamete attachment requires GEX2 for successful fertilization in *Arabidopsis*. *Curr Biol* **24**: 170–175
- Mori T, Kuroiwa H, Higashiyama T, Kuroiwa T** (2006) GENERATIVE CELL SPECIFIC 1 is essential for angiosperm fertilization. *Nat Cell Biol* **8**: 64–71



- Palanivelu R, Preuss D** (2006) Distinct short-range ovule signals attract or repel *Arabidopsis thaliana* pollen tubes in vitro. *BMC Plant Biol* **6**: 7
- Pleskot R, Pejchar P, Bezdova R, Lichtscheidl IK, Wolters-Arts M, Marc J, Žárský V, Potocký M** (2012) Turnover of phosphatidic acid through distinct signaling pathways affects multiple aspects of pollen tube growth in tobacco. *Front Plant Sci* **3**: 54
- Qin Y, Leydon AR, Manziello A, Pandey R, Mount D, Denic S, Vasic B, Johnson MA, Palanivelu R** (2009) Penetration of the stigma and style elicits a novel transcriptome in pollen tubes, pointing to genes critical for growth in a pistil. *PLoS Genet* **5**: e1000621
- Reyes FC, Buono RA, Roschztardt H, Di Rubbo S, Yeun LH, Russinova E, Otegui MS** (2014) A novel endosomal sorting complex required for transport (ESCRT) component in *Arabidopsis thaliana* controls cell expansion and development. *J Biol Chem* **289**: 4980–4988
- Ruiz MT, Voinnet O, Baulcombe DC** (1998) Initiation and maintenance of virus-induced gene silencing. *Plant Cell* **10**: 937–946
- Ryder SP, Recht MI, Williamson JR** (2008) Quantitative analysis of protein-RNA interactions by gel mobility shift. *Methods Mol Biol* **488**: 99–115
- Samaj J, Müller J, Beck M, Böhm N, Menzel D** (2006) Vesicular trafficking, cytoskeleton and signalling in root hairs and pollen tubes. *Trends Plant Sci* **11**: 594–600
- Scarpin MR, Sigaut L, Temprana SG, Boccaccio GL, Pietrasanta LI, Muschietti JP** (2017) Two *Arabidopsis* late pollen transcripts are detected in cytoplasmic granules. *Plant Direct* **1**: e00012
- Schulz-Raffelt M, Chochois V, Auroy P, Cuiné S, Billon E, Dauvillée D, Li-Beisson Y, Peltier G** (2016) Hyper-accumulation of starch and oil in a *Chlamydomonas* mutant affected in a plant-specific DYRK kinase. *Biotechnol Biofuels* **9**: 55
- Stålberg K, Ståhl U, Stymne S, Ohlrogge J** (2009) Characterization of two *Arabidopsis thaliana* acyltransferases with preference for lysophosphatidylethanolamine. *BMC Plant Biol* **9**: 60
- Synek L, Schlager N, Eliáš M, Quentin M, Hauser M-T, Žárský V** (2006) AtEXO70A1, a member of a family of putative exocyst subunits specifically expanded in land plants, is important for polar growth and plant development. *Plant J* **48**: 54–72
- Synek L, Vukašinović N, Kulich I, Hála M, Aldorfová K, Fendrych M, Žárský V** (2017) EXO70C2 is a key regulatory factor for optimal tip growth of pollen. *Plant Physiol* **174**: 223–240
- Takemoto K, Ebine K, Askani JC, Krüger F, Gonzalez ZA, Ito E, Goh T, Schumacher K, Nakano A, Ueda T** (2018) Distinct sets of tethering complexes, SNARE complexes, and Rab GTPases mediate membrane fusion at the vacuole in *Arabidopsis*. *Proc Natl Acad Sci USA* **115**: E2457–E2466
- Tian L, Chou H-L, Fukuda M, Kumamaru T, Okita TW** (2020) mRNA localization in plant cells. *Plant Physiol* **182**: 97–109
- Töpfer R, Matzeit V, Gronenborn B, Schell J, Steinbiss HH** (1987) A set of plant expression vectors for transcriptional and translational fusions. *Nucleic Acids Res* **15**: 5890
- Tse YC, Lo SW, Hillmer S, Dupree P, Jiang L** (2006) Dynamic response of prevacuolar compartments to brefeldin A in plant cells. *Plant Physiol* **142**: 1442–1459
- Twell D, Wing R, Yamaguchi J, McCormick S** (1989) Isolation and expression of an anther-specific gene from tomato. *Mol Gen Genet* **217**: 240–245
- van der Veen JH, Wirtz P** (1968) EMS-induced genic male sterility in *Arabidopsis thaliana*: a model selection experiment. *Euphytica* **17**: 371–377
- Voigt B, Timmers ACJ, Samaj J, Müller J, Baluska F, Menzel D** (2005) GFP-FABD2 fusion construct allows in vivo visualization of the dynamic actin cytoskeleton in all cells of *Arabidopsis* seedlings. *Eur J Cell Biol* **84**: 595–608
- Vukašinović N, Žárský V** (2016) Tethering complexes in the *Arabidopsis* endomembrane system. *Front Cell Dev Biol* **4**: 46
- Vukmirovic M, Manojlovic Z, Stefanovic B** (2013) Serine-threonine kinase receptor-associated protein (STRAP) regulates translation of type I collagen mRNAs. *Mol Cell Biol* **33**: 3893–3906
- Weber C, Nover L, Fauth M** (2008) Plant stress granules and mRNA processing bodies are distinct from heat stress granules. *Plant J* **56**: 517–530
- Weng H, Kim C, Valavanis C, Wang Z, Schwartz LM** (2009) Acheron, an novel LA antigen family member, binds to CASK and forms a complex with Id transcription factors. *Cell Mol Biol Lett* **14**: 273–287
- Woody ST, Austin-Phillips S, Amasino RM, Krysan PJ** (2007) The WiscDsLox T-DNA collection: an *Arabidopsis* community resource generated by using an improved high-throughput T-DNA sequencing pipeline. *J Plant Res* **120**: 157–165
- Ylstra B, McCormick S** (1999) Analysis of mRNA stabilities during pollen development and in BY2 cells. *Plant J* **20**: 101–108
- Yu J, Qiu H, Liu X, Wang M, Gao Y, Chory J, Tao Y** (2015) Characterization of tub4(P287L), a  $\beta$ -tubulin mutant, revealed new aspects of microtubule regulation in shade. *J Integr Plant Biol* **57**: 757–769
- Zhang M, Fan J, Taylor DC, Ohlrogge JB** (2009) DGAT1 and PDAT1 acyltransferases have overlapping functions in *Arabidopsis* triacylglycerol biosynthesis and are essential for normal pollen and seed development. *Plant Cell* **21**: 3885–3901
- Zhang Y, Stefanovic B** (2016) LARP6 meets collagen mRNA: specific regulation of type I collagen expression. *Int J Mol Sci* **17**: 419
- Zheng Y, Deng X, Qu A, Zhang M, Tao Y, Yang L, Liu Y, Xu J, Zhang S** (2018) Regulation of pollen lipid body biogenesis by MAP kinases and downstream WRKY transcription factors in *Arabidopsis*. *PLoS Genet* **14**: e1007880
- Zhou J-J, Liang Y, Niu Q-K, Chen L-Q, Zhang X-Q, Ye D** (2013) The *Arabidopsis* general transcription factor TFIIIB1 (AtTFIIIB1) is required for pollen tube growth and endosperm development. *J Exp Bot* **64**: 2205–2218